Entanglement spectrum and Rényi entropies of nonrelativistic conformal fermions

William J. Porter* and Joaquín E. Drut†

Department of Physics and Astronomy, University of North Carolina, Chapel Hill, North Carolina 27599-3255, USA

(Received 30 May 2016; revised manuscript received 6 September 2016; published 6 October 2016)

We characterize nonperturbatively the Rényi entropies of degree $n = 2$, 3, 4, and 5 of three-dimensional, strongly coupled many-fermion systems in the scale-invariant regime of short interaction range and large scattering length, i.e., in the unitary limit. We carry out our calculations using lattice methods devised recently by us. Our results show the effect of strong pairing correlations on the entanglement entropy, which modify the subleading behavior for large subsystem sizes (as characterized by the dimensionless parameter $x = k_F L_A$, where k_F is the Fermi momentum and L_A the linear subsystem size), but leave the leading order unchanged relative to the noninteracting case. Moreover, we find that the onset of the subleading asymptotic regime is at surprisingly small $x \simeq 2$–4. We provide further insight into the entanglement properties of this system by analyzing the spectrum of the entanglement Hamiltonian of the two-body problem from weak to strong coupling. The low-lying entanglement spectrum displays clear features as the strength of the coupling is varied, such as eigenvalue crossing and merging, a sharp change in the Schmidt gap, and scale invariance at unitarity. Beyond the low-lying component, the spectrum appears as a quasicontinuum distribution, for which we present a statistical characterization; we find, in particular, that the mean shifts to infinity as the coupling is turned off, which indicates that that part of the spectrum represents nonperturbative contributions to the entanglement Hamiltonian. In contrast, the low-lying entanglement spectrum evolves to finite values in the noninteracting limit. The scale invariance of the unitary regime guarantees that our results are universal features intrinsic to three-dimensional quantum mechanics and represent a well-defined prediction for ultracold atom experiments, which were recently shown to have direct access to the entanglement entropy.

DOI: 10.1103/PhysRevB.94.165112

I. INTRODUCTION

This is an incredibly exciting time for research in ultracold atomic physics. The degree of control that experimentalists have achieved continues to rise, year after year, along with their ability to measure collective properties in progressively more ingenious ways (see, e.g. [1–4]). Indeed, after the realization of Bose-Einstein condensates over two decades ago [5–7] (see also [8]), followed by Fermi condensates in 2004 [9], the field entered an accelerated phase and rapidly developed control of multiple parameters such as temperature, polarization, and interaction strength (in alkali gases via Feshbach resonances, see, e.g. [10], and more recently in alkaline-earth gases via orbital resonances, see, e.g. [11–13]), as well as exquisite tuning of external trapping potentials. Additionally, multiple properties can be measured, ranging from the equation of state (see, e.g. [14–16]) to hydrodynamic response (see, e.g. [17,18]) and, more recently, the entanglement entropy [19,20].

This sustained progress has strengthened the intersections with other areas of physics, in particular modern condensed matter physics and quantum information [21], as well as with nuclear [22] and particle physics [23–25]. Quantum simulation by fine manipulation of nuclear spins, electronic states, and optical lattices, now appears more realistic than ever [26–28]. At the interface between many of those areas lies a deceptively simple nonrelativistic scale invariant system: the unitary Fermi gas, which corresponds to the limit of vanishing interaction range r_0 and infinite s-wave scattering length a, i.e.,

$$0 \leftarrow r_0 \ll n^{-1} \ll a \rightarrow \infty, \tag{1}$$

where n is the density; this regime corresponds to the threshold of two-body bound-state formation.

Both a model for dilute neutron matter and an actually realized resonant atomic gas, this universal spin-1/2 system has brought together the nuclear [29–32], atomic [33], and condensed matter physics areas [34–36], as well as the AdS/CFT area [37–39], due to the underlying nonrelativistic conformal invariance [40]. While many properties of this quintessential many-body problem are known (see, e.g. [22] for an extensive review), other properties like entanglement and quantum information aspects have thus far remained unexplored, which brings us to our main point.

As this work is being written, quantum information concepts are increasingly becoming part of the modern language of quantum many-body physics (see, e.g., Refs. [21,41–43]), in particular with regards to the characterization of topological phases of matter and quantum computation, but also in connection with black holes (see, e.g. [44]) and string theory (see, e.g. [45]). In the past decade or so, a large body of work has been produced characterizing the entanglement properties of low dimensional systems (especially those with spin degrees of freedom [46–48]) at quantum phase transitions (in particular those with topological order parameters that defy a local description) as well as systems of noninteracting fermions and bosons [49–53], which presented a challenge of their own.

With that new perspective in mind, in this work we set out to characterize the entanglement properties of the unitary Fermi gas using nonperturbative lattice methods. We analyze the reduced density matrix, entanglement spectrum, and associated Rényi entanglement entropies of the two-body problem by implementing an exact projection technique on the lattice. For the many-body problem, we use a Monte Carlo method developed by us in Refs. [54,55], based on the work of

*wjporter@live.unc.edu
†drut@email.unc.edu

Ref. [56], to calculate the nth Rényi entanglement entropy. We showed in that work that our method overcomes the signal-to-noise problem of naive Monte Carlo approaches. We did that using the 1D Fermi-Hubbard model as a test case, but to our knowledge no previous calculations have been attempted for the challenging case of 3D Fermi gases.

The remainder of this paper is organized as follows. In Sec. II we present the main definitions and set the stage for Sec. III, where we explain how we carry out our calculations of the entanglement spectrum and entanglement entropies in two- and many-fermion systems. For completeness, we also include in that section a discussion on how to avoid the signal-to-noise issue that plagues entanglement-entropy calculations in the many-body case. We extend that discussion to the case of bosons in the same section. In Sec. IV we show our results for the entanglement spectrum and entropies of the two-body system along the BCS-BEC crossover, and in Sec. V we present the Rényi entanglement entropies of many fermions at unitarity. We present a summary and our main conclusions in Sec. VI. The Appendixes contain more detailed explanations of our few- and many-body methods.

II. DEFINITIONS: HAMILTONIAN, DENSITY MATRICES, AND THE ENTANGLEMENT ENTROPY

The Hamiltonian governing the dynamics of resonant fermions can be written as

$$\hat{H} = \hat{T} + \hat{V}, \tag{2}$$

where the nonrelativistic kinetic energy operator is

$$\hat{T} = \sum_{s=\uparrow,\downarrow} \int d^3r\, \hat{\psi}_s^\dagger(\mathbf{r}) \left(-\frac{\nabla^2}{2m}\right) \hat{\psi}_s(\mathbf{r}), \tag{3}$$

where $\hat{\psi}_s^\dagger(\mathbf{r})$ and $\hat{\psi}_s(\mathbf{r})$ are the creation and annihilation operators of particles of spin $s = \uparrow, \downarrow$ at location $\mathbf{r}$.

The two-body, zero-range interaction operator is

$$\hat{V} = -g \int d^3r\, \hat{\psi}_\uparrow^\dagger(\mathbf{r}) \hat{\psi}_\uparrow(\mathbf{r}) \hat{\psi}_\downarrow^\dagger(\mathbf{r}) \hat{\psi}_\downarrow(\mathbf{r}), \tag{4}$$

where the bare coupling g is tuned to the desired physical situation. By definition, the limit of unitarity is achieved by requiring that the ground state of the two-body problem lies at the threshold of bound-state formation (note that in 1D and 2D bound states form at arbitrarily small attractive coupling, but a finite value is required in 3D). Because our work was carried out in a finite volume with periodic boundary conditions, we used Lüscher's formalism [57,58] to relate the bare coupling to the scattering length in the analysis of the BCS-BEC crossover. We describe that procedure below, when showing the results for the two-body problem.

The full, normalized density matrix of the system is

$$\hat{\rho} = \frac{e^{-\beta \hat{H}}}{\mathcal{Q}}, \tag{5}$$

where

$$\mathcal{Q} = \mathrm{Tr}_{\mathcal{H}}[e^{-\beta \hat{H}}] \tag{6}$$

is of course the canonical partition function, and $\mathcal{H}$ is the full Hilbert space. In this work we are concerned with systems in a pure state, namely the ground state $|\Xi\rangle$, such that the full density matrix can be written as

$$\hat{\rho} = |\Xi\rangle\langle\Xi|. \tag{7}$$

Both in the few- and many-body systems we analyze here, the ground-state density matrix will be approached by a projection method we describe below.

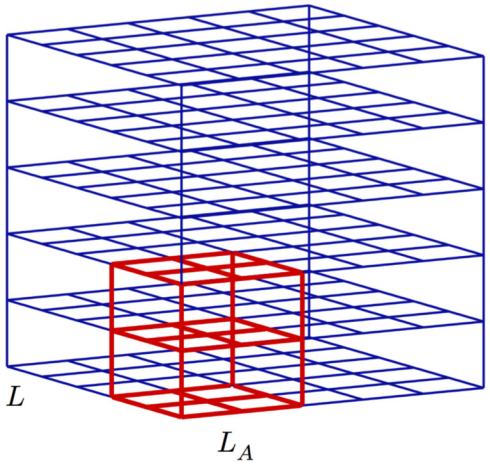

FIG. 1. (Bipartite) entanglement entropies computed in this work correspond to partitioning the system into a subsystem A (in coordinate space, but it can also be defined in momentum space) and its complement $\bar{A}$. In practice, the calculations are carried out on systems that live in a cubic lattice of side L, and the subsystems are defined by cubic subregions of side $L_A \leqslant L$. The reduced density matrix $\hat{\rho}_A$ of the open system A contains the information about entanglement between A and $\bar{A}$, and is obtained by tracing the full density matrix over the states supported by $\bar{A}$, which form the Hilbert space $\mathcal{H}_{\bar{A}}$.

A subsystem A and its complement $\bar{A}$ (in coordinate or momentum space; see Fig. 1) support states that belong to Hilbert spaces $\mathcal{H}_A$ and $\mathcal{H}_{\bar{A}}$, respectively, such that the Hilbert space $\mathcal{H}$ of the full system can be written as a direct product space

$$\mathcal{H} = \mathcal{H}_A \otimes \mathcal{H}_{\bar{A}}. \tag{8}$$

The density matrix $\hat{\rho}_A$ of subsystem A, usually referred to as the reduced density matrix, is defined by tracing over the degrees of freedom supported by $\bar{A}$, i.e., tracing over the states in $\mathcal{H}_{\bar{A}}$:

$$\hat{\rho}_A = \mathrm{Tr}_{\mathcal{H}_{\bar{A}}} \hat{\rho}. \tag{9}$$

Based on this definition, the properties of A as an open subsystem can be formulated and computed using operators with support in A. In particular, a quantitative measure of entanglement between A and $\bar{A}$ is given by the von Neumann entanglement entropy,

$$S_{\mathrm{vN},A} = -\mathrm{Tr}_{\mathcal{H}_A}[\hat{\rho}_A \ln \hat{\rho}_A], \tag{10}$$

and by the nth order Rényi entanglement entropy,

$$S_{n,A} = \frac{1}{1-n} \ln \mathrm{Tr}_{\mathcal{H}_A}\left[\hat{\rho}_A^n\right]. \tag{11}$$

Naturally, these entropies vanish when A is the whole system, as then there is full knowledge of the state of the system.

In any other case, the entanglement entropy will be nonzero, unless the ground state factorizes into a state living in A and a state living in $\bar{A}$. Because the entanglement between A and $\bar{A}$ happens across the boundary that separates those regions, it is natural to expect $S_{n,A}$ to be extensive with the size of that boundary, i.e., proportional to the area delimiting A. This point was the topic of many papers in the past decade or so, especially in connection with quantum phase transitions (see, e.g. [59]).

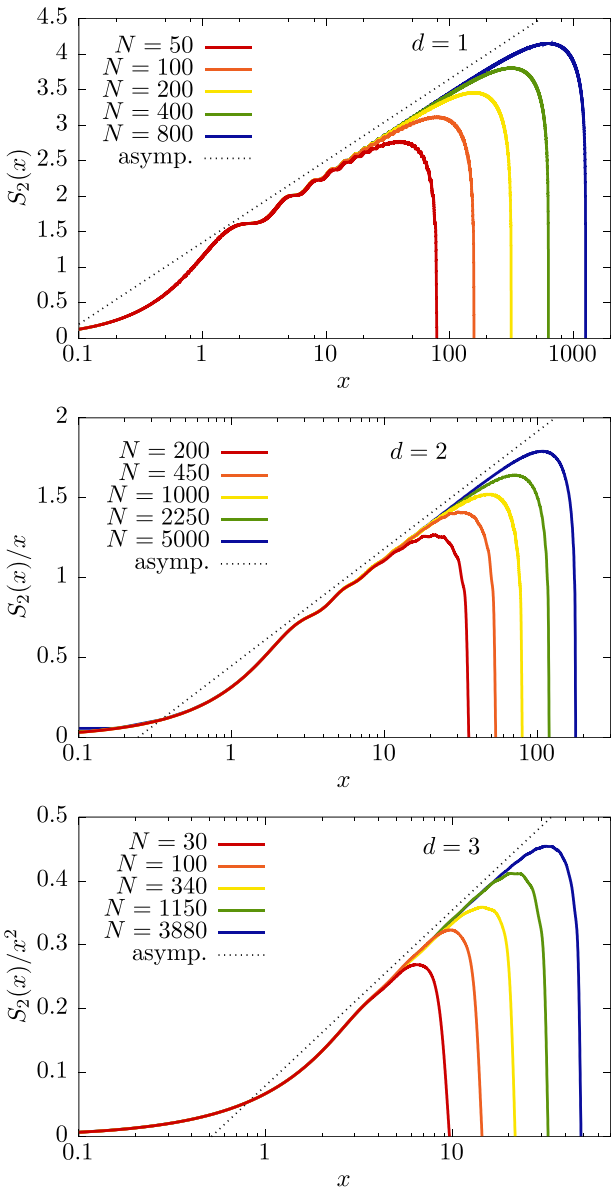

FIG. 2. Second Rényi entropy S_2 of N noninteracting fermions in $d = 1,2,3$ dimensions (top to bottom) as a function of $x = k_F L_A$, where A is a segment, square, and cubic region, respectively, and L_A is the corresponding linear size; k_F is the Fermi momentum. S_2 is scaled by the surface area dependence, namely x and x^2 in 2D and 3D, respectively. The x axis is plotted logarithmically to show that, up to finite-size effects, the results heal to the expected asymptotic regime of linear dependence with $\log_{10} x$ (dashed line). This regime sets in at $x \simeq 2$–4 across all d. Finite-size effects appear as a sudden drop at large x.

It was rigorously shown in recent years, however, that the Rényi entropy of noninteracting fermions with a well-defined Fermi surface presents a logarithmic violation of the area law [49–53]. This abnormality was confirmed numerically with the aid of overlap-matrix methods [60], which we reproduce in Fig. 2, where we explicitly show said logarithmic dependence (dashed line) as a function of $x = k_F L_A$, where k_F is the Fermi momentum and L_A is the linear size of region A, such that

$$x = k_F L_A = \frac{\pi N}{2}\frac{L_A}{L} \quad \text{in 1D}, \tag{12}$$

$$= (2\pi N)^{1/2}\frac{L_A}{L} \quad \text{in 2D}, \tag{13}$$

$$= (3\pi^2 N)^{1/3}\frac{L_A}{L} \quad \text{in 3D}, \tag{14}$$

where N is the total particle number. Note that, at large enough x, finite size effects eventually take over and the entropy quickly tends to zero. The subleading oscillations were studied in detail in Ref. [61].

Although resonant fermions are strongly coupled (the regime is nonperturbative and away from any regime with small dimensionless parameters), we can expect $S_{n,A}$ to follow a similar trend as the noninteracting gas, for the following reasons. First, resonant fermions have a distinguishable Fermi surface (note, however, that that is quickly lost as one proceeds towards the BEC side of the resonance), whose role in the entanglement entropy has been emphasized many times (see, e.g. [62]). Second, our experience with $S_{n,A}$ for the Hubbard model in other cases [54] indicates that very strong couplings U/t are needed even in 1D (where quantum fluctuations are qualitatively stronger than in 3D) in order for $S_{n,A}$ to noticeably depart from the noninteracting result. Thus we anticipate a similar behavior for resonant fermions as that of the bottom panel of Fig. 2; the latter provides some qualitative knowledge of where the leading logarithmic and subleading dependence sets in for $S_{n,A}$ as a function of $x = k_F L_A$. In fact, as we will see below, the onset of the asymptotic behavior (meaning dominated by leading and subleading dependence on x) at $x \simeq 2$–4 is the same for unitarity as for the noninteracting case. This is surprising, as there is no obvious reason for that to be the case: had this onset appeared at $x \simeq 10$, the calculations in this work would not have been possible, as they would have required huge lattices. We return to this discussion below, when presenting our results for the many-body case.

III. METHOD

In this section we explain the two approaches used in this work. We address the two-body problem first, which we solved with a direct (i.e., nonstochastic) projection method on the lattice (See Fig. 3). This problem can be solved exactly by changing to center-of-mass and relative coordinates. However, doing so implies using a method that only works in that case, and we are interested in techniques that can be used in a variety of situations (e.g., in the presence of external fields, more than two particles, time-dependent cases, and so forth). We then address the many-body problem using a method recently

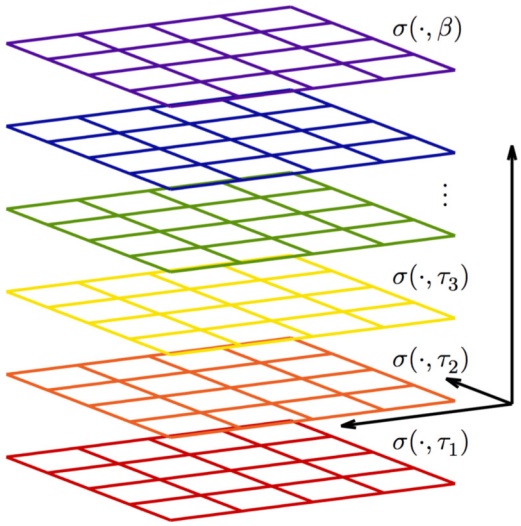

FIG. 3. Shown here is a representation of the lattice used in our calculations. Each horizontal lattice plane represents the 3D lattice where the system lives, and the vertical stacking of the planes represents the imaginary time direction. Although the original Hamiltonian is time independent, the auxiliary field σ that represents the interaction is supported by a spacetime lattice and induces a time dependence that disappears upon averaging.

put forward by us, which we first presented and tested for one-dimensional systems in Ref. [55].

Although both approaches make use of an auxiliary field transformation, the ultimate utility of this technique is markedly different in each case. We detail below the portion of the formalism common to both approaches, treating in subsequent sections the details of their divergence from common assumptions and notation.

At chemical potential μ and inverse temperature β, the grand canonical partition function $\mathcal{Z}$ is defined via

$$\mathcal{Z} = \mathrm{Tr}\,[e^{-\beta(\hat{H}-\mu\hat{N})}] \tag{15}$$

for Hamiltonian $\hat{H}$ and particle-number operator $\hat{N}$. Writing the inverse temperature as an integer number N_τ of steps, we implement a symmetric Suzuki-Trotter decomposition with the goal of separating each operator into distinct one- and two-body factors. For the Boltzmann factor, we obtain

$$e^{-\beta(\hat{H}-\mu\hat{N})} = \prod_{j=1}^{N_\tau} e^{-\tau\hat{K}/2}e^{-\tau\hat{V}}e^{-\tau\hat{K}/2} + \mathcal{O}(\tau^2), \tag{16}$$

where we define

$$\hat{K} = \hat{T} - \mu\hat{N}. \tag{17}$$

At each position $\mathbf{r}$ and for each of the N_τ factors, we decompose the interaction via the introduction of a Hubbard-Stratonovich auxiliary field σ which we choose to be of a continuous and compact form [63,64]. More specifically for each space-time position $(\mathbf{r},\tau_j)$, where $\mathbf{r}\in[0,L)^3$ and $\tau_j = j\tau$ for some $1\leqslant j\leqslant N_\tau$, we write

$$e^{\tau g\hat{n}_\uparrow\hat{n}_\downarrow} = \int_{-\pi}^{\pi}\frac{d\sigma}{2\pi}(\mathbb{1} + B\,\hat{n}_\uparrow\sin\sigma)(\mathbb{1} + B\,\hat{n}_\downarrow\sin\sigma) \tag{18}$$

having suppressed the space-time dependence of the field σ and the spatial dependence of the fermion density operators $\hat{n}_s(\mathbf{r}) = \hat{\psi}_s^\dagger(\mathbf{r})\hat{\psi}_s(\mathbf{r})$ where $s=\uparrow,\downarrow$. Knowing that $\hat{n}_s(\mathbf{r})$ is idempotent, it follows that

$$e^{\tau g\hat{n}_\uparrow\hat{n}_\downarrow} = 1 + (e^{\tau g}-1)\hat{n}_\uparrow\hat{n}_\downarrow, \tag{19}$$

which shows that the constant B satisfies

$$e^{\tau g} - 1 = \frac{B^2}{2}. \tag{20}$$

Collecting the integration measures, we obtain a path-integral form of the partition function accurate to quadratic order in the temporal lattice spacing, writing

$$\mathcal{Z} = \int \mathcal{D}\sigma\,\mathrm{Tr}\,\hat{\mathcal{U}}[\sigma] + \mathcal{O}(\tau^2), \tag{21}$$

where

$$\hat{\mathcal{U}}[\sigma] = \prod_{j=1}^{N_\tau}\hat{\mathcal{U}}_j[\sigma], \tag{22}$$

and the individual factors are

$$\hat{\mathcal{U}}_j[\sigma] = e^{-\tau\hat{K}/2}\prod_{\mathbf{r}}(\mathbb{1} + B\,\hat{n}_\uparrow(\mathbf{r})\sin\sigma(\mathbf{r},\tau_j)) \tag{23}$$

$$\times(\mathbb{1} + B\,\hat{n}_\downarrow(\mathbf{r})\sin\sigma(\mathbf{r},\tau_j))e^{-\tau\hat{K}/2}. \tag{24}$$

As the kinetic energy operator $\hat{T}$ and the number operator $\hat{N}$ are already written as products of flavor-specific operators, we may partition the operator $\hat{\mathcal{U}}$ into individual factors each of which assumes responsibility for the evolution of a particular fermion species $s=\uparrow,\downarrow$. We do this by defining operators $\hat{T}_s$, $\hat{N}_s$, and $\hat{K}_s$ for $s=\uparrow,\downarrow$ by

$$\hat{T}_s = \int d^3r\,\hat{\psi}_s^\dagger(\mathbf{r})\left(-\frac{\nabla^2}{2m}\right)\hat{\psi}_s(\mathbf{r}), \tag{25}$$

$$\hat{N}_s = \int d^3r\,\hat{\psi}_s^\dagger(\mathbf{r})\hat{\psi}_s(\mathbf{r}), \tag{26}$$

and $\hat{K}_s = \hat{T}_s - \mu\hat{N}_s$. We then write

$$\hat{\mathcal{U}}_{j,s}[\sigma] = e^{-\tau\hat{K}_s/2}\prod_{\mathbf{r}}(\mathbb{1} + B\,\hat{n}_s(\mathbf{r})\sin\sigma(\mathbf{r},\tau_j))e^{-\tau\hat{K}_s/2}, \tag{27}$$

such that

$$\hat{\mathcal{U}}[\sigma] = \hat{\mathcal{U}}_\uparrow[\sigma]\,\hat{\mathcal{U}}_\downarrow[\sigma], \tag{28}$$

where

$$\hat{\mathcal{U}}_s[\sigma] = \prod_{j=1}^{N_\tau}\hat{\mathcal{U}}_{j,s}[\sigma]. \tag{29}$$

Performing the required Fock-space trace, the exponential form of each factor in the above provides (see, e.g. [65])

$$\mathcal{Z} = \int \mathcal{D}\sigma\ \det(\mathbb{1} + \boldsymbol{U}_\uparrow[\sigma])\det(\mathbb{1} + \boldsymbol{U}_\downarrow[\sigma]), \tag{30}$$

where we have suppressed higher-order contributions in τ (which are of order τ^2), and written a matrix $\boldsymbol{U}_s[\sigma]$ for the restriction of each of the operators $\hat{\mathcal{U}}_s[\sigma]$ to the single-particle

Hilbert space. Each of those matrices contains an overall factor of the fugacity

$$z \equiv e^{\beta\mu}. \tag{31}$$

In what follows, we exhibit this factor explicitly and redefine the matrices $\boldsymbol{U}_s[\sigma]$ to reflect this revision. In this work, we exclusively treat unpolarized systems, and so we may treat the determinants as equivalent in derivations that follow by writing

$$\mathcal{Z} = \int \mathcal{D}\sigma \, \det{}^2(\mathbb{1} + z\,\boldsymbol{U}[\sigma]), \tag{32}$$

and neglecting to denote the spin degree of freedom wherever context precludes confusion.

A. Direct lattice approach to the entanglement spectrum of the two-body problem

1. *Identifying the transfer matrix*

In order to illustrate the details as well as the generality of our technique, we show the main steps here in broad strokes and leave the details for Appendix A.

Using the above path-integral form of $\mathcal{Z}$, we first isolate the two-body sector. From the finite-temperature partition function Eq. (30), we may derive the conventional virial expansion in powers of the fugacity for each spin, which is given by

$$\mathcal{Z} = \sum_{N_\uparrow, N_\downarrow = 0}^{\infty} z_\uparrow^{N_\uparrow} z_\downarrow^{N_\downarrow} \mathcal{Q}_{N_\uparrow, N_\downarrow}, \tag{33}$$

where we have identified the coefficient of the N_sth power of the fugacity as the N_s-particle canonical partition function $\mathcal{Q}_{N_\uparrow, N_\downarrow}$. Expanding the path-integral expression for the grand canonical partition function, we find that in terms of the matrix $\boldsymbol{U}[\sigma]$, the $(1+1)$-particle partition function is

$$\mathcal{Q}_{1,1} = \int \mathcal{D}\sigma \, \mathrm{tr}^2 \, \boldsymbol{U}[\sigma]. \tag{34}$$

The path integral in $\mathcal{Q}_{1,1}$ above can be evaluated directly in a way that elucidates the form of the two-body transfer matrix. To that end, we define a four-index object from which the above squared trace may be obtained by suitable index contraction:

$$R_{ab,cd} = \int \mathcal{D}\sigma \, \boldsymbol{U}[\sigma]_{ac} \boldsymbol{U}[\sigma]_{bd}. \tag{35}$$

The same four-index object, with indices properly contracted to account for antisymmetry, can be used to analyze the $(2+0)$-particle case.

We next write out each of the matrices $\boldsymbol{U}[\sigma]$ in its product form; that is, we reintroduce Eq. (22) in matrix form:

$$\boldsymbol{U}[\sigma] = \prod_{j=1}^{N_\tau} \boldsymbol{U}_j[\sigma]. \tag{36}$$

For each contribution to the N-body transfer matrix, exactly N factors of the matrix $\boldsymbol{U}[\sigma]$ appear, and as a result each temporal lattice point appears in the integrand N times. Turning to the individual factors, we write each of the matrices $\boldsymbol{U}_j[\sigma]$ in such a way as to exhibit the interaction. That is, we write

$$\boldsymbol{U}_j[\sigma] = \boldsymbol{T}\boldsymbol{V}_j[\sigma]\boldsymbol{T}, \tag{37}$$

where

$$[\boldsymbol{T}]_{\mathbf{k}\mathbf{k}'} = e^{-(\tau/2)k^2/2}\delta_{\mathbf{k},\mathbf{k}'} \tag{38}$$

is the single-particle form of the kinetic energy operator defined above (in momentum space), and the (position-space representation of the) auxiliary external potential operator has matrix elements

$$[\boldsymbol{V}_j[\sigma]]_{\mathbf{r}\mathbf{r}'} = (1 + B\,\sin\sigma(\mathbf{r},\tau_j))\delta_{\mathbf{r}\mathbf{r}'}. \tag{39}$$

At this point, all matrix elements have been written out and can be shifted around as needed to carry out the path integral. The only nonzero results are obtained, of course, when an even number (in this $N=2$ case no more than 2) of fields $\sigma(\mathbf{r},\tau_j)$ appear in the integrand for the same values of $(\mathbf{r},\tau_j)$.

This undoing of the Hubbard-Stratonovich transformation may seem a cumbersome or convoluted way to proceed, but it is useful in that it mechanically generates the correct expression for the N-body partition function for *any* particle content simply by differentiation of the fermion determinants. Moreover, this is accomplished without the need to deal with operator algebra and is easily generalized to bosons. In the two-body case, in particular, the above procedure results in

$$R_{ac,bd} = \left[M_2^{N_\tau}\right]_{ac,bd}, \tag{40}$$

where we have naturally identified the transfer matrix in the two-particle subspace

$$[M_2]_{ac,bd} = \mathcal{K}_{ab}\mathcal{K}_{cd} + (e^{\tau g} - 1)\mathcal{I}_{abcd}, \tag{41}$$

and where

$$\mathcal{K}_{ij} = \sum_p \boldsymbol{T}_{ip}\boldsymbol{T}_{pj}, \tag{42}$$

$$\mathcal{I}_{ijkl} = \sum_p \boldsymbol{T}_{ip}\boldsymbol{T}_{pj}\boldsymbol{T}_{kp}\boldsymbol{T}_{pl}. \tag{43}$$

The form of the transfer matrix lends itself to a useful diagrammatic representation, which we show for the two- and three-particle cases (the latter derived in Appendix A) in Eqs. (44), (45), and (46):

$[M_2]_{ac,bd}$ = 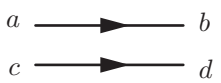

$+ \quad (e^{\tau g} - 1)$ 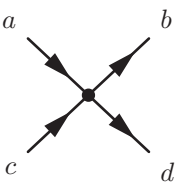

(44)

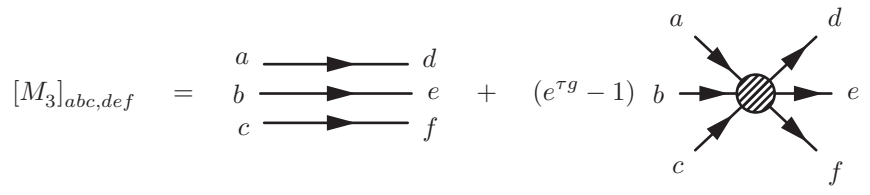

(45)

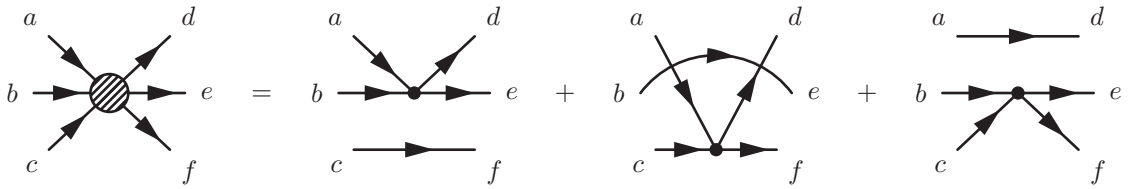

(46)

2. *Obtaining the ground state and the reduced density matrix*

Having identified the transfer matrix allows us to design a projection method to approach the ground state by repeated application of M_2. Proposing a guess state $|\Xi_0\rangle$, we extract the true two-particle ground state $|\Xi\rangle$ via

$$M_2^{N_\tau}|\Xi_0\rangle \xrightarrow{N_\tau\to\infty} |\Xi\rangle. \tag{47}$$

In practice, we compute the position-space wave function $\xi(x_\uparrow,x_\downarrow)=\langle x_\uparrow,x_\downarrow|\Xi\rangle$. Wave function in hand, we compute the matrix elements of the full density matrix $\hat\rho$ as

$$\langle x_\uparrow,x_\downarrow|\,\hat\rho\,|x'_\uparrow,x'_\downarrow\rangle = \langle x_\uparrow,x_\downarrow|\Xi\rangle\langle\Xi|x'_\uparrow,x'_\downarrow\rangle \tag{48}$$

$$= \xi^*(x'_\uparrow,x'_\downarrow)\,\xi(x_\uparrow,x_\downarrow). \tag{49}$$

From these, the elements of the reduced density matrix $\hat\rho_A$ can be obtained as well. Given two states $|s\rangle,|s'\rangle\in\mathcal{H}_A$ for the subregion A, each state being specified by choosing for each particle either a position in A or in the complement $\bar A$, we compute

$$\langle s|\,\hat\rho_A\,|s'\rangle = \sum_{a\in\mathcal{A}_{ss'}} (|s\rangle\otimes|a\rangle)^\dagger\,\hat\rho\,(|s'\rangle\otimes|a\rangle), \tag{50}$$

where, at each fixed pair of two-particle states s,s', the sum is taken over all states $|a\rangle\in\mathcal{H}_{\bar A}$ such that the state $|s\rangle\otimes|a\rangle\in\mathcal{H}_A\otimes\mathcal{H}_{\bar A}$ ($|s'\rangle\otimes|a\rangle\in\mathcal{H}_A\otimes\mathcal{H}_{\bar A}$) is consistent with the first (second) index of the matrix element being evaluated. We have denoted this set as $\mathcal{A}_{ss'}$. From this matrix, we compute the entanglement spectrum $\sigma(\hat H_A)$, that is the spectrum of the entanglement Hamiltonian defined

$$\hat\rho_A = e^{-\hat H_A}, \tag{51}$$

as well as the von Neumann and Rényi entanglement entropies.

B. Lattice Monte Carlo approach to the many-body problem

To address the many-body system, we implement the Monte Carlo version of the algorithm outlined above. The output of this algorithm, however, is not the ground-state wave function but rather the expectation value of the desired observable in a projected state. In our case, the observable is of course the entanglement entropy. To obtain it, crucial intermediate steps are required that go beyond conventional Monte Carlo approaches. We therefore outline the basic formalism first, and then proceed to explain the additional steps required to calculate $S_{n,A}$.

1. *Basic formalism*

Beginning with a largely arbitrary many-body state $|\Omega_0\rangle$, we evolve the state forward in imaginary time by an extent β via

$$|\Omega(\beta)\rangle = e^{-\beta\hat H}|\Omega_0\rangle. \tag{52}$$

For large imaginary times, we have

$$|\Omega(\beta)\rangle \xrightarrow{\beta\to\infty} |\Omega\rangle, \tag{53}$$

where $|\Omega\rangle$ is the true ground state provided that $\langle\Omega_0|\Omega\rangle\neq 0$.

For an operator $\hat O$, we may obtain the ground-state expectation value by studying the asymptotic behavior of the function

$$O(\beta) = \frac{1}{Z(\beta)}\langle\Omega(\beta/2)|\,\hat O\,|\Omega(\beta/2)\rangle, \tag{54}$$

with the zero-temperature normalization defined as

$$Z(\beta) = \langle\Omega(\beta/2)|\Omega(\beta/2)\rangle = \langle\Omega_0|\,e^{-\beta\hat H}\,|\Omega_0\rangle. \tag{55}$$

As derived in detail earlier, we implement a symmetric factorization of the Boltzmann weight [cf. Eq. (16)] in order to separate factors depending only on the one-body kinetic-energy operator from the significantly more complicated two-body potential-energy operator responsible for the effects of the interaction. Following this approximation, we again implement an auxiliary field transformation [cf. Eq. (18)] to represent the interaction factor. This allows us to write the ground-state estimator of Eq. (54) defined above in path integral form as

$$O(\beta) = \frac{1}{Z(\beta)}\int \mathcal{D}\sigma\; P_\beta[\sigma]\; O_\beta[\sigma], \tag{56}$$

while simultaneously demonstrating that

$$Z(\beta) = \int \mathcal{D}\sigma\; P_\beta[\sigma]. \tag{57}$$

We have identified a naturally emerging probability measure $P_\beta[\sigma]$ computed as

$$P_\beta[\sigma] = \langle\Omega_0|\,\hat{\mathcal{U}}_\beta[\sigma]\,|\Omega_0\rangle, \tag{58}$$

with the operator $\hat{\mathcal{U}}_\beta[\sigma]$ defined as in Eq. (22) (setting $\mu = 0$ in the kinetic energy factor since particle number is fixed in this formalism). The integrand takes the form

$$O_\beta[\sigma] = \frac{\langle\Omega_0|\hat{\mathcal{U}}_{\beta/2}[\sigma]\,\hat{O}\,\hat{\mathcal{U}}_{\beta/2}[\sigma]\,|\Omega_0\rangle}{\langle\Omega_0|\hat{\mathcal{U}}_\beta[\sigma]\,|\Omega_0\rangle}. \tag{59}$$

Taking advantage of the arbitrariness of the initial state, we choose for $|\Omega_0\rangle$ a Slater determinant for each fermion species constructed from single-particle plane-wave states ϕ_j for $1 \leqslant j \leqslant N/2$ with $N/2 = N_\downarrow = N_\uparrow$. With this assumption, we find that the probability takes the form

$$P_\beta[\sigma] = \det{}^2\boldsymbol{U}_\beta[\sigma], \tag{60}$$

with

$$[\boldsymbol{U}_\beta[\sigma]]_{kk'} = \langle\phi_k|\hat{\mathcal{U}}_\beta[\sigma]\,|\phi_{k'}\rangle, \tag{61}$$

where the indices k,k' satisfy $1 \leqslant k,k' \leqslant N/2$.

2. *Path integral form of the reduced density matrix, replica fields, and the Rényi entropy*

It was shown by Grover in Ref. [56] that the reduced density matrix can be written in terms of the fermionic creation and annihilation operators $\hat{c}^\dagger,\hat{c}$ as a weighted average with respect to the probability measure $P_\beta[\sigma]$ derived above. Specifically,

$$\hat{\rho}_{A,\beta} = \int \mathcal{D}\sigma\; P_\beta[\sigma]\;\hat{\rho}_{A,\beta}[\sigma], \tag{62}$$

where

$$\hat{\rho}_{A,\beta}[\sigma] = \det\left(\mathbb{1} - G_{A,\beta}[\sigma]\right) \times \exp\left(-\sum_{i,j\in A}\hat{c}_i^\dagger\left[\log\left(G_{A,\beta}^{-1}[\sigma] - \mathbb{1}\right)\right]_{ij}\hat{c}_j\right). \tag{63}$$

It is important to note that $\hat{\rho}_{A,\beta}[\sigma]$ is the reduced density matrix of a system of noninteracting fermions in the external field σ. Expressions for noninteracting reduced density matrices were first derived in Refs. [66–68], but it was not until the much more recent work of Ref. [56] that those were combined into the nonperturbative form of Eq. (62) amenable to Monte Carlo calculations.

In the above, $G_{A,\beta}[\sigma]$ is the spatial restriction of the (equal-time) one-body density matrix for either flavor to the region A computed as

$$G_{A,\beta}[\sigma]_{rr'} = \sum_{a,b=1}^{N/2}[\boldsymbol{U}_\beta^{-1}[\sigma]]_{ab}\phi_b^*(r,\beta/2)\phi_a(r',\beta/2), \tag{64}$$

where

$$\phi_a(r',\beta/2) = \langle r'|\hat{\mathcal{U}}_\beta[\sigma]|\phi_a\rangle, \tag{65}$$

$$\phi_b^*(r,\beta/2) = \langle\phi_b|\hat{\mathcal{U}}_\beta[\sigma]|r\rangle. \tag{66}$$

We suppress the imaginary-time β dependence in much of what follows with the understanding that calculations are to be performed in the limit of $\beta \to \infty$.

From this decomposed form of the reduced density matrix, an estimator for the nth order Rényi entropy can be derived. Because n powers of $\hat{\rho}_A$ are needed, an equal number of auxiliary fields will appear (the "replica" fields), which we will denote collectively as $\boldsymbol{\sigma}$.

The final result (see Refs. [54–56,69,70]) takes the form

$$\exp((1-n)S_{n,A}) = \mathrm{Tr}_{\mathcal{H}_A}\left[\rho_A^n\right] = \frac{1}{Z^n}\int \mathcal{D}\Sigma\; P[\boldsymbol{\sigma}]\; Q[\boldsymbol{\sigma}], \tag{67}$$

where (note the suppressed β dependence)

$$P[\boldsymbol{\sigma}] = P[\sigma_1]P[\sigma_2]\ldots P[\sigma_n], \tag{68}$$

with the observable being

$$Q[\boldsymbol{\sigma}] = \det{}^2 W[\boldsymbol{\sigma}], \tag{69}$$

with

$$W[\boldsymbol{\sigma}] = \prod_{j=1}^{n}(\mathbb{1} - G_A[\sigma_j])\left[\mathbb{1} + \prod_{k=1}^{n}\frac{G_A[\sigma_k]}{\mathbb{1} - G_A[\sigma_k]}\right]. \tag{70}$$

We have adopted a notation such that, for functions or integrals of functions of multiple auxiliary fields, we write

$$F[\boldsymbol{\sigma}] = F[\sigma_1,\sigma_2,\ldots,\sigma_n] \tag{71}$$

and

$$\int \mathcal{D}\Sigma\; F[\boldsymbol{\sigma}] = \int \mathcal{D}\sigma_1\mathcal{D}\sigma_2\ldots\mathcal{D}\sigma_n\; F[\boldsymbol{\sigma}], \tag{72}$$

respectively.

Equation (70) poses the challenging task of inverting $\mathbb{1} - G_A$, which can be very nearly singular, as pointed out in Ref. [69]. For $n = 2$, no inversion is required, because the equations simplify such that

$$Q[\boldsymbol{\sigma}] = \det{}^2[(\mathbb{1} - G_A[\sigma_1])(\mathbb{1} - G_A[\sigma_2]) + G_A[\sigma_1]G_A[\sigma_2]]. \tag{73}$$

However, for higher n there is no simplification of that kind and therefore it is less clear how one may avoid the problem. We solved this problem in Ref. [55] (see also [71–74]); the main point is realizing that

$$\det\; W[\boldsymbol{\sigma}] = \det\; L[\boldsymbol{\sigma}]\;\det\; K[\boldsymbol{\sigma}], \tag{74}$$

where $L[\boldsymbol{\sigma}]$ is a block diagonal matrix (one block per replica k):

$$L[\boldsymbol{\sigma}] \equiv \mathrm{diag}[\mathbb{1} - G_A[\sigma_k]], \tag{75}$$

and

$$K[\boldsymbol{\sigma}] \equiv \begin{pmatrix} \mathbb{1} & 0 & 0 & \ldots & 0 & -R[\sigma_n] \\ R[\sigma_1] & \mathbb{1} & 0 & \ldots & \vdots & 0 \\ 0 & R[\sigma_2] & \mathbb{1} & 0 & 0 & 0 \\ \vdots & \ddots & \ddots & \ddots & \mathbb{1} & \vdots \\ 0 & \ldots & \ldots & 0 & R[\sigma_{n-1}] & \mathbb{1} \end{pmatrix}, \tag{76}$$

where

$$R[\sigma_k] = \frac{G_A[\sigma_k]}{G_A[\sigma_k] - \mathbb{1}}. \tag{77}$$

Within the determinant of Eq. (74), we multiply $K[\boldsymbol{\sigma}]$ and $L[\boldsymbol{\sigma}]$ and define

$$T[\boldsymbol{\sigma}] \equiv K[\boldsymbol{\sigma}]L[\boldsymbol{\sigma}] = \mathbb{1} - D\,\mathcal{G}[\boldsymbol{\sigma}], \tag{78}$$

where $\mathcal{G}[\boldsymbol{\sigma}]$ is a block diagonal matrix defined by

$$\mathcal{G}[\boldsymbol{\sigma}] = \mathrm{diag}[G_A[\sigma_k]], \tag{79}$$

and

$$D \equiv \begin{pmatrix} \mathbb{1} & 0 & 0 & \dots & -\mathbb{1} \\ \mathbb{1} & \mathbb{1} & 0 & \dots & 0 \\ 0 & \mathbb{1} & \mathbb{1} & \dots & 0 \\ \vdots & \ddots & \ddots & \ddots & \vdots \\ 0 & \dots & 0 & \mathbb{1} & \mathbb{1} \end{pmatrix}. \tag{80}$$

Equation (83) is the result that allows us to bypass the inversion of $\mathbb{1} - G_A$. Moreover, the form of $T[\boldsymbol{\sigma}]$ is clearly simpler than that of $W[\boldsymbol{\sigma}]$. For those reasons we use $T[\boldsymbol{\sigma}]$ in all of the many-body calculations presented here. This formulation allowed us to study Rényi entropies as high as $n = 5$; higher are also possible.

For completeness, we present here the simplification for the bosonic case as well (and add a subindex B accordingly), for which

$$Q_B[\boldsymbol{\sigma}] = \det{}^{-2} W_B[\boldsymbol{\sigma}] \tag{81}$$

and

$$W_B[\boldsymbol{\sigma}] = \prod_{j=1}^{n}(\mathbb{1} + G_A[\sigma_j])\left[\mathbb{1} - \prod_{k=1}^{n}\frac{G_A[\sigma_k]}{\mathbb{1} + G_A[\sigma_k]}\right]. \tag{82}$$

The analogous strategy to avoid inversion leads here to

$$T_B[\boldsymbol{\sigma}] \equiv \mathbb{1} - D_B\mathcal{G}[\boldsymbol{\sigma}], \tag{83}$$

where $\mathcal{G}[\boldsymbol{\sigma}]$ is a block diagonal matrix defined by

$$\mathcal{G}[\boldsymbol{\sigma}] = \mathrm{diag}[G_A[\sigma_n]], \tag{84}$$

and

$$D_B \equiv \begin{pmatrix} -\mathbb{1} & 0 & 0 & \dots & \mathbb{1} \\ \mathbb{1} & -\mathbb{1} & 0 & \dots & 0 \\ 0 & \mathbb{1} & -\mathbb{1} & \dots & 0 \\ \vdots & \ddots & \ddots & \ddots & \vdots \\ 0 & \dots & 0 & \mathbb{1} & -\mathbb{1} \end{pmatrix}. \tag{85}$$

3. *Signal-to-noise issues and how to overcome them*

The path integral form of the Rényi entropy Eq. (67) has a deceptively simple form: it seems obvious that one should interpret $P[\boldsymbol{\sigma}]$ as the probability density and $Q[\boldsymbol{\sigma}]$ as the observable being averaged. This, in some sense, is a trap: while $Q[\boldsymbol{\sigma}]$ is crucially sensitive to correlations among the replica fields σ_k, $P[\boldsymbol{\sigma}]$ completely factorizes across replicas (i.e., it is insensitive to said correlations). As a consequence, a Monte Carlo implementation sampling $\boldsymbol{\sigma}$ according to $P[\boldsymbol{\sigma}]$ will give outlandish values of $Q[\boldsymbol{\sigma}]$ that fluctuate wildly and may not converge to the expected value. This feature is what in the lattice QCD area is often called an overlap problem (see, e.g., Refs. [75,76]). The present case is especially challenging in 2D and 3D, as the magnitude of $Q[\boldsymbol{\sigma}]$ is expected to grow exponentially with the size of the boundary of the subregion A (see, e.g. [71,72]).

Motivated by the similarity between the numerator of Eq. (67) and the conventional path-integral form of partition functions, we address the overlap problem by first differentiating with respect to a parameter, then using Monte Carlo methods to compute that derivative, and finally integrating at the end. We outline this procedure in detail in Ref. [55], and reproduce part of it here.

We introduce a parameter $0 \leqslant \lambda \leqslant 1$ by defining a function $\Gamma(\lambda; g)$ such that

$$\Gamma(\lambda; g) \equiv \int \mathcal{D}\Sigma\; P[\boldsymbol{\sigma}]Q^{\lambda}[\boldsymbol{\sigma}]. \tag{86}$$

Normalization of $P[\boldsymbol{\sigma}]$ implies that

$$\ln\Gamma(0; g) = 0, \tag{87}$$

while Eq. (67) implies

$$\ln\Gamma(1; g) = (1-n)S_{n,A}. \tag{88}$$

Using Eq. (86),

$$\frac{\partial\,\ln\Gamma}{\partial\lambda} = \int \mathcal{D}\Sigma\;\tilde{P}[\boldsymbol{\sigma};\lambda]\ln Q[\boldsymbol{\sigma}], \tag{89}$$

where

$$\tilde{P}[\boldsymbol{\sigma};\lambda] \equiv \frac{1}{\Gamma(\lambda; g)}P[\boldsymbol{\sigma}]\;Q^{\lambda}[\boldsymbol{\sigma}] \tag{90}$$

is a well-defined, normalized probability measure which features the usual weight $P[\boldsymbol{\sigma}]$ as well as an entanglement contribution $Q^{\lambda}[\boldsymbol{\sigma}]$. It is the latter factor that induces entanglement-specific correlations in the sampling of $\boldsymbol{\sigma}$ when probability $\tilde{P}[\boldsymbol{\sigma};\lambda]$.

Thus $S_{n,A}$ is calculated by using $\lambda = 0$ as a reference point and computing $S_{n,A}$ via

$$S_{n,A} = \frac{1}{1-n}\int_0^1 d\lambda\langle\ln Q[\boldsymbol{\sigma}]\rangle_{\lambda}, \tag{91}$$

where

$$\langle X\rangle_{\lambda} = \int \mathcal{D}\Sigma\;\tilde{P}[\boldsymbol{\sigma};\lambda]\;X[\boldsymbol{\sigma}]. \tag{92}$$

We thus obtain an integral form of the interacting Rényi entropy that can be computed using any MC method (see, e.g. [63–65]), in particular hybrid Monte Carlo [77,78] to tackle the evaluation of $\langle\ln Q[\boldsymbol{\sigma}]\rangle_{\lambda}$ as a function of λ. In practice, we find that $\langle\ln Q[\boldsymbol{\sigma}]\rangle_{\lambda}$ is a smooth function of λ, as exemplified in Fig. 4. It is therefore sufficient to perform the numerical integration using a uniform grid.

IV. RESULTS: TWO-BODY SYSTEM

We solve the two-body problem via the projection method outlined previously, which furnishes the full two-body wave function on the lattice. We ensure that the continuum limit is approached by solving the problem for multiple lattice sizes, and by computing the renormalized coupling using the energy spectrum and Lüscher's formalism [57,58]. The latter indicates that the relationship between the energy eigenvalues and the scattering phase shift $\delta(p)$ is given by

$$p\,\cot\delta(p) = \frac{1}{\pi L}\mathcal{S}(\eta), \tag{93}$$

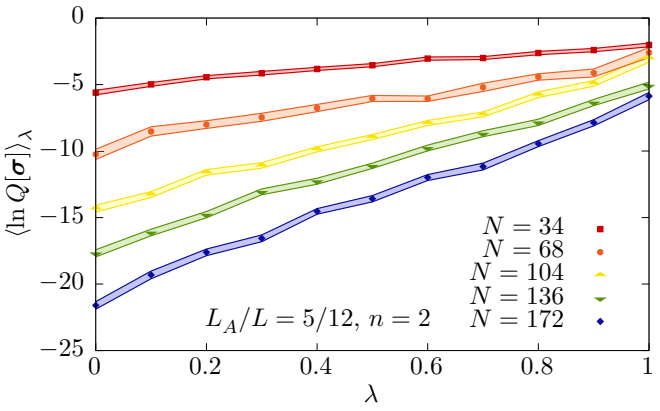

FIG. 4. λ dependence of $\langle \ln Q[\sigma] \rangle_\lambda$ for a subsystem of size $L_A = 5/12L$, for $N = 34,68,104,136,172$ fermions at unitarity in a box of size $L = N_x \ell$ (where $N_x = 12$ points and $\ell = 1$), and for Rényi order $n = 2$. Similar plots are obtained by varying, instead of the particle number, the region size and the Rényi order. These are shown in Appendix B.

where $\eta = \frac{pL}{2\pi}$ and L is the box size, such that the energy of the two-body problem is $E = p^2/m$; and

$$\mathcal{S}(\eta) \equiv \lim_{\Lambda\to\infty} \left(\sum_{\mathbf{n}} \frac{\Theta(\Lambda^2 - \mathbf{n}^2)}{\mathbf{n}^2 - \eta^2} - 4\pi\Lambda \right), \tag{94}$$

where the sum is over all 3D integer vectors, and $\Theta(x)$ is the Heaviside function. In turn, the scattering phase shift determines the scattering parameters via

$$p\ \cot\delta(p) = -\frac{1}{a} + \frac{1}{2} r_{\text{eff}} p^2 + O(p^4), \tag{95}$$

where δ is the scattering phase shift, a is the scattering length, and r_{eff} is the effective range.

A. Low-lying entanglement spectrum

Once the matrix elements of $\hat{\rho}_A$ are calculated from the projected ground state, as shown above, we obtain the eigenvalues using standard diagonalization routines to obtain the entanglement spectrum $\sigma(\hat{H}_A)$, which is defined as the spectrum of the entanglement Hamiltonian $\hat{H}_A$, where

$$\hat{\rho}_A = e^{-\hat{H}_A}. \tag{96}$$

In Fig. 5, we present our results for $\sigma(\hat{H}_A)$ for a cubic subregion A of linear size $L_A/L = 0.5$, for two particles in the BCS-BEC crossover, parametrized by the dimensionless coupling $(k_F a)^{-1}$, where k_F is the Fermi momentum (merely a measure of the particle density in the periodic box, as for two particles there is of course no Fermi surface) and a is the s-wave scattering length. The latter was determined using the Lüscher formalism outlined above.

The main features of $\sigma(\hat{H}_A)$ can be described as follows. We note first that beyond the lowest four or five eigenvalues, shown as λ_1 to λ_5 in the bottom panel of Fig. 5, the multiplicity of eigenvalues grows dramatically, forming a quasicontinuum. For this reason, we focus here on the lowest five eigenvalues and characterize the rest statistically in the next section. As is evident from the figure, the dependence of all λ_k on $(k_F a)^{-1}$

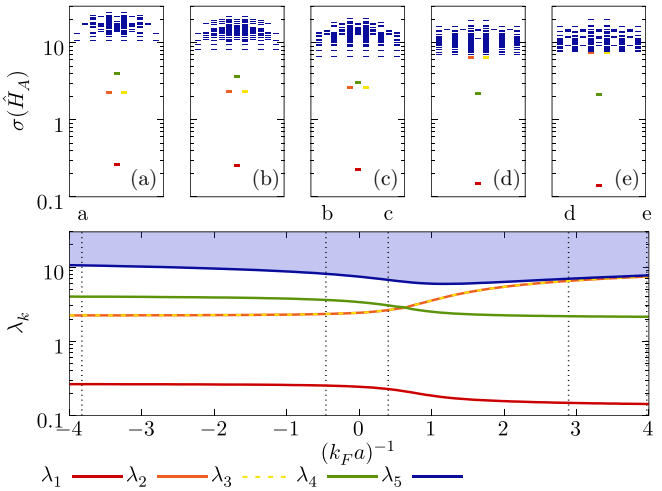

FIG. 5. Bottom panel: low-lying entanglement spectrum of the two-body problem as a function of the dimensionless coupling $(k_F a)^{-1}$ in the BCS-BEC crossover, for a cubic subregion A of linear size $L_A/L = 0.5$. Top panels [(a)–(e)]: low-lying (and part of the high) entanglement spectrum for selected couplings [(a)–(e)] at the top of the bottom panel.

is rather mild and smooth, although it has a few crisp features: there is a rather large gap between λ_1 and the next eigenvalue, which implies that the Rényi entanglement entropies are dominated by that eigenvalue; there is a crossing of λ_2, λ_3, and λ_4 on the BEC side of the resonance; after that crossing λ_2 and λ_3 heal to λ_5 and effectively merge into the lower edge of the quasicontinuum part of the spectrum. The evolution of these properties along the crossover is shown in detail in panels (a)–(e) of Fig. 5.

In Fig. 6 we show the Schmidt gap Δ (see Ref. [79]), defined as the separation between the two largest eigenvalues of the reduced density matrix $\hat{\rho}_A$, for $L_A/L = 0.1,0.2,\ldots,0.5$, as a function of $(k_F a)^{-1}$. Since we do not expect a quantum phase transition as a function of $(k_F a)^{-1}$, we similarly do not expect the Schmidt gap to vanish. As a result of the eigenvalue crossing explained above, however, there exists a sharp change

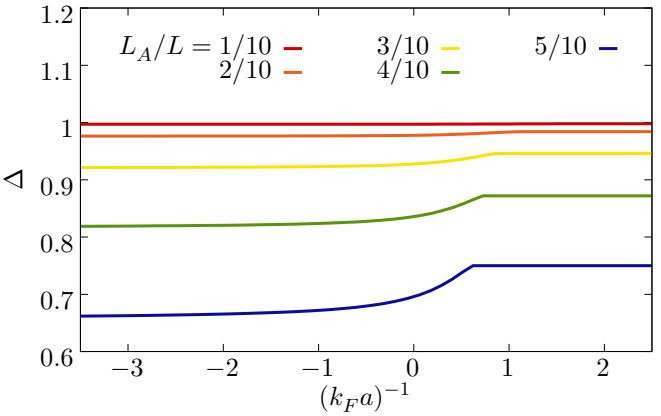

FIG. 6. Schmidt gap Δ between the two largest eigenvalues of the reduced density matrix, at $L_A/L = 0.1,0.2,\ldots,0.5$ (top to bottom), for the two-body system as a function of the coupling $(k_F a)^{-1}$.

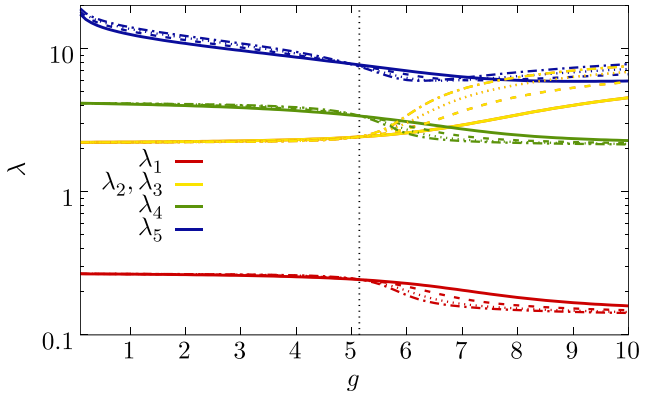

FIG. 7. Entanglement spectrum of the two-body problem in the BCS-BEC crossover as a function of the bare lattice coupling at different lattice sizes: solid, dashed, dotted, dash-dotted, for $N_x = 4,6,8,10$, respectively. The subsystem size was fixed to $L_A/L = 0.5$. The coupling corresponding to the unitary point is marked with a vertical dashed line. Note how different volumes cross precisely at unitarity, which reflects the property of scale invariance.

(in the sense of a discontinuous derivative) in Δ in the BCS-BEC crossover, which takes place in the strongly coupled region $0 < (k_F a)^{-1} < 1$. It is also evident that, because λ_1 and λ_4 track each other at a very nearly constant separation, the Schmidt gap becomes constant to the right of the sharp edge in Fig. 6. As with other features of this spectrum, it remains to be determined how Δ evolves as a function of particle number, in particular as a Fermi surface forms and Cooper pairing correlations emerge.

As mentioned above, our calculations were carried out in a periodic box. We show the corresponding size effects in Fig. 7, where we show the entanglement spectrum of the two-body system as a function of the bare lattice coupling g. In that figure, it is clear that finite-size effects are smallest on the BCS side of the resonance, but become considerably more important on the BEC side. This is consistent with the expectation that, once a two-body bound state forms (as the coupling is increased away from the noninteracting point), the sensitivity to lattice-spacing effects is enhanced. It is noteworthy, in particular, that one may identify the unitary regime just by looking at this figure: for any given eigenvalue, the data for different lattice sizes crosses at about the same value of g; this is reminiscent of the finite-size scaling behavior of order parameters in critical phenomena, as it is the hallmark of scale invariance at phase transitions.

The process of reducing finite-size effects, at fixed particle number, implies approaching the dilute limit, i.e., using larger lattices. When that limit is approached, the renormalization prescription that replaces g with the physical coupling $(k_F a)^{-1}$ (described above) should force the finite-size calculations to collapse to a single, universal (in the sense of size-independent) curve. This is indeed what we find and what yields the results of Fig. 5.

B. High entanglement spectrum

As mentioned in the previous section, the entanglement spectrum $\sigma(\hat{H}_A)$ above λ_5, which we will refer to here as the high entanglement spectrum, displays a rapidly growing multiplicity of eigenvalues which we deem best to analyze using elementary statistical methods. In Fig. 8, we show the eigenvalue distribution of the high entanglement spectrum for different system sizes, in histogram form. More importantly, we find that the mean and standard deviation of that distribution, shown here in Fig. 8 (middle and bottom), are smooth functions of $(k_F a)^{-1}$; the mean, in particular, diverges as the coupling is turned off. We interpret this effect as strong evidence that the high sector of $\sigma(\hat{H}_A)$ is a nonperturbative component of $\hat{H}_A$ that is entirely due to

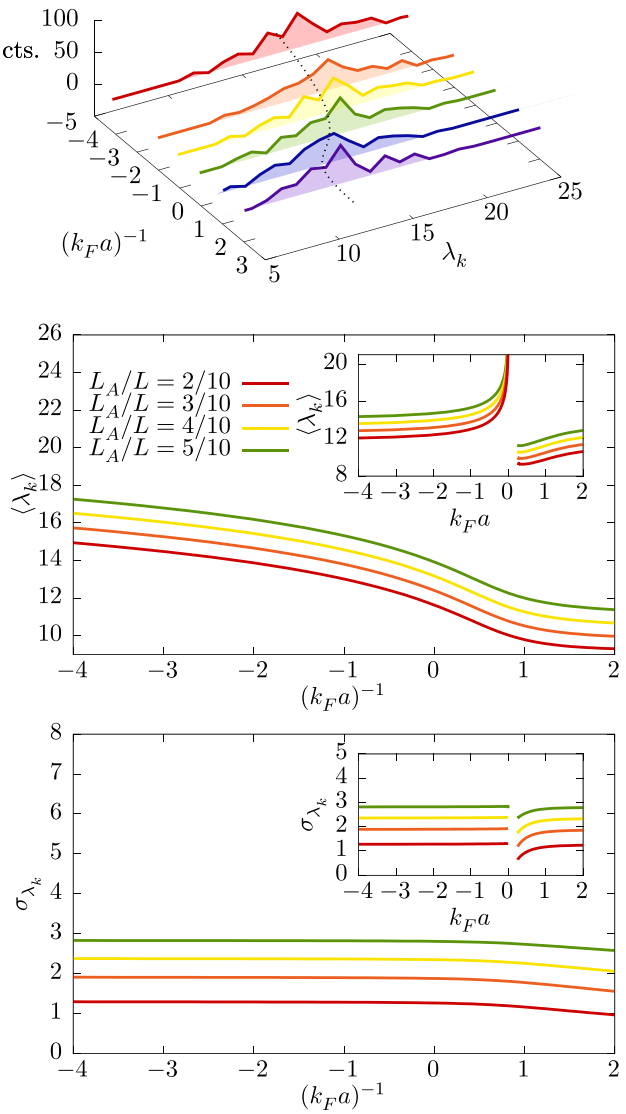

FIG. 8. Top: histogram of the high entanglement spectrum of the two-body problem showing number of counts (cts) as a function of the coupling $(k_F a)^{-1}$ and the entanglement eigenvalue λ_k, for region size $L_A/L = 1/2$. The dashed line shows the dependence of the mean (see also middle plot). Middle and bottom: Mean and standard deviation, respectively, of the high entanglement spectrum distribution, as functions of the interaction strength $(k_F a)^{-1}$ (main) and $k_F a$ (inset). In each plot the different curves show results for various L_A/L. Note that the weak coupling limit corresponds to $k_F a \to 0^-$.

quantum fluctuations induced by the interaction. Although the two-body system has no Fermi surface, it seems natural to conjecture a link between Cooper pairing and the high entanglement spectrum. Determining whether this is true, however, is a challenging problem that requires studying the high entanglement spectrum in the progression from few to many particles.

Our numerical calculations show a large number of eigenvalues that lie far (at least 9 to 10 orders of magnitude) above the high entanglement spectrum. While we cannot discard that those eigenvalues are consistent with numerical noise (they come from the lowest eigenvalues of the reduced density matrix), there are enough of them to warrant this brief comment. Although there is a large number of such eigenvalues, their contribution to the entanglement entropy is considerably suppressed by their small magnitude. We add to this discussion below.

C. Entanglement entropy

Using our knowledge of the eigenvalues $\lambda_k \in \sigma(\hat{H}_A)$, the entanglement entropy of the two-body problem is easily determined. Indeed, the von Neumann entropy is

$$S_{\mathrm{vN},A} = -\mathrm{Tr}_{\mathcal{H}_A}[\hat{\rho}_A \ln \hat{\rho}_A] = \sum_k \lambda_k \, e^{-\lambda_k}, \tag{97}$$

and the nth order Rényi entanglement entropy is

$$S_{n,A} = \frac{1}{1-n} \ln \mathrm{Tr}_{\mathcal{H}_A}\left[\hat{\rho}_A^n\right] = \frac{1}{1-n} \ln \sum_k e^{-n\lambda_k}. \tag{98}$$

In Fig. 9 (top panel), we show S_2 as a function of $x = k_F L_A$ and the coupling $(k_F a)^{-1}$. Remarkably, the trend towards the leading asymptotic behavior proportional to $x^2 \ln x$ appears to set in at $x \simeq 2$ for all couplings. This is surprising, as there is no obvious reason for this to be the case. As we will see below, we find the same kind of behavior for the many-body Fermi gas at resonance.

To show explicitly the effect of the high entanglement spectrum on S_2, which we referred to in the previous section, we show in Fig. 9 (bottom panel) the contribution ΔS_2 of the first entanglement eigenvalue to the full S_2. It is clear in that plot that the contribution is at most on the order of 8% for the parameter ranges we studied.

V. RESULTS: MANY-BODY SYSTEM

Using the many-body lattice Monte Carlo techniques described above, along with the tuning procedure outlined in the previous section, we computed several entanglement entropies of the unitary Fermi gas, aiming to characterize its leading and subleading asymptotic behavior as a function of the subregion size $x = k_F L_A$.

The results shown throughout this section were obtained by gathering 250 decorrelated auxiliary field configurations (where a single "auxiliary field" contains all the replicas required to determine the desired Rényi entropy) for each value of the auxiliary parameter λ. We used particle numbers in the range $N = 4$–400 and cubic lattice sizes in the range $N_x = 6$–16 with periodic boundary conditions. The projection to the ground state was carried out by extrapolation to the limit

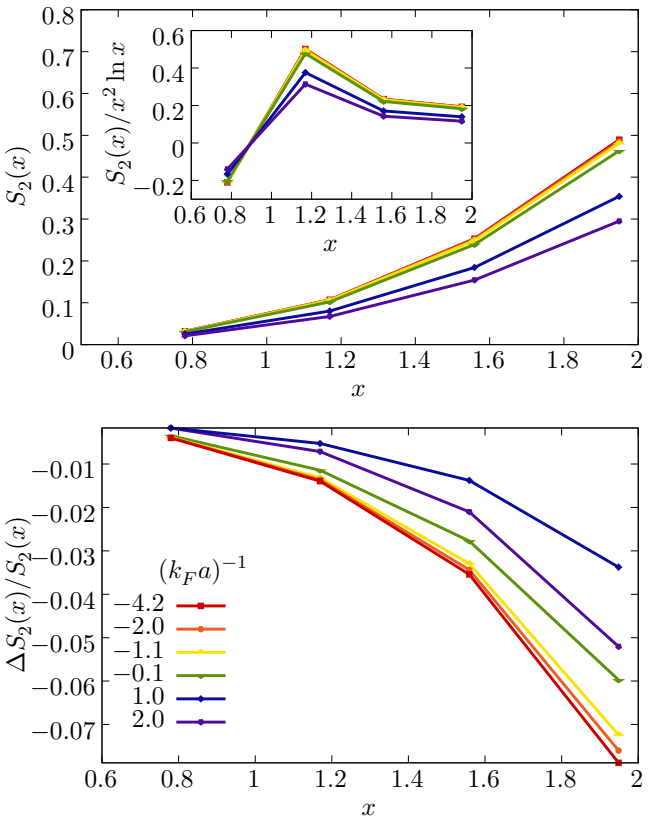

FIG. 9. Top: second Rényi entanglement entropy S_2 of the two-body problem as a function of $x = k_F L_A$ and for several values of the coupling $(k_F a)^{-1}$. Inset: S_2 scaled by $x^2 \ln x$. Bottom: relative contribution of the high entanglement spectrum to the second Rényi entanglement entropy S_2, as a function of $x = k_F L_A$.

of large imaginary-time direction. The auxiliary parameter λ was discretized using $N_\lambda = 10$ points, which we found to be enough to capture the very mild dependence on that parameter, as explained in a previous section (see also Appendix B for further details).

Because the methods we implemented impose a discretization of space-time, special attention was given to the ordering of the scales, to ensure that the thermodynamic and continuum limit were approached. Specifically, we required the following ordering:

$$k_F \ell \ll 1 \ll k_F L_A \ll k_F L, \tag{99}$$

where $\ell = 1$ is the lattice spacing, L_A is the subsystem size, and $L = N_x \ell = N_x$ is the full system size. The first condition on the left of Eq. (99) ensures that the continuum limit is approached; the second condition implies that the region determined by L_A must contain many particles (since the density is the only scale in the system, this condition defines the large-L_A regime); and the last condition means that $L_A \ll L$, to ensure finite-size effects are minimized. This ordering was accomplished by carefully choosing the restrictions on L_A for a given particle number N, while aiming to maintain a large N. The latter, however, requires L to be large in order to avoid high densities where $k_F \simeq 1$, which can be sensitive to lattice-spacing effects. In addition, we set $L_A \leqslant 0.45L$ as a compromise to satisfy the last inequality.

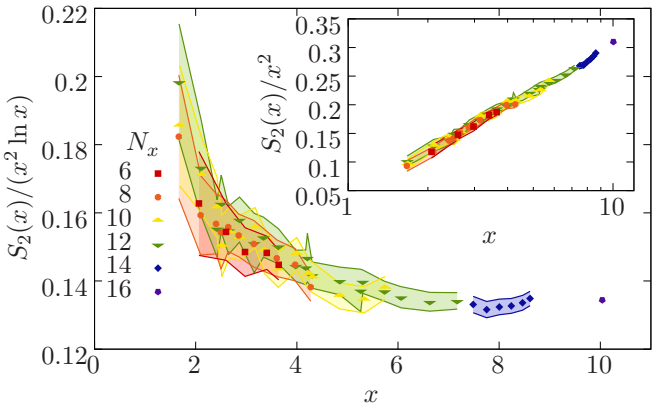

FIG. 10. Second Rényi entropy of the unitary Fermi gas in units of $x^2 \ln x$ (main) and x^2 (inset), where $x = k_F L_A$. Note the linear scale in the main plot and logarithmic scale in the inset. Although the range of values of x is limited by our computational power (as set by method and hardware), the fact that the main plot is consistent with a straight line is a strong indication that the leading behavior of the entanglement entropy as a function of x is logarithmic. Moreover, we see that that behavior sets in as early as $x \simeq 2$, which is roughly consistent with the noninteracting case shown in Fig. 2.

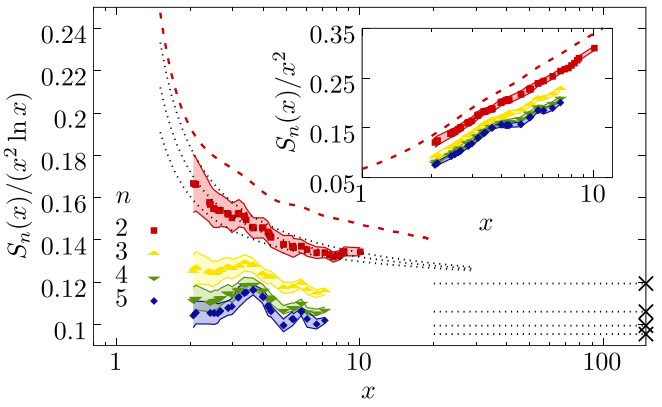

FIG. 11. Rényi entropies of order $n = 2,3,4,5$ (data points with error bands in red, yellow, green, and blue, respectively) of the unitary Fermi gas in units of $x^2 \ln x$ (main plot) and x^2 (inset), where $x = k_F L_A$. Note the logarithmic scale in the x axis. The red dashed line shows the noninteracting result for $n = 2$, obtained using the overlap matrix method. The black dotted lines plotted over the $n = 2$ data correspond to fit the functional form $f(x) = a + b/\ln(x)$ (central line, with uncertainties marked by upper and lower dotted lines). The crosses on the right, and the corresponding horizontal dotted lines, indicate the expected asymptotic value $c(n)$ (from top to bottom, for $n = 2,3,4,5$) for a noninteracting gas (see Refs. [49–53]), which we reproduce in Eq. (101); numerically, they are $c(2) = 0.11937\ldots$, $c(3) = 0.10610\ldots$, $c(4) = 0.09947\ldots$, and $c(5) = 0.09549\ldots$.

In Fig. 10 we show our results of the second Rényi entropy S_2 of the unitary Fermi gas in volumes of N_x^3 lattice points, where $N_x = 6$–16, as a function of $x = k_F L_A$, for cubic subsystems of side L_A. Within the statistical uncertainty, shown in colored bands, the results for different volumes coincide, which indicates that our results are in the continuum and thermodynamic regimes.

The inset of Fig. 10 shows S_2 scaled by x^2 in a semilog plot. The fact that the trend is clearly linear supports the assertion that x is large enough to discern the asymptotic regime, where $S_2/x^2 \propto \ln x$. As in the case of the noninteracting Fermi gas, mentioned in the Introduction, this onset of the asymptotic regime appears to be at $x \simeq 2$.

A. Rényi entanglement entropies

Using the formalism presented above for the determination of Rényi entanglement entropies for $n \geqslant 2$, we computed $S_{n,A}$ for the resonant Fermi gas for $n = 2,3,4,5$, as a function of $x = k_F L_A$. In Fig. 11 we show our main results. To interpret those results, we briefly discuss the noninteracting case. In Refs. [49–53] it was shown that the leading-order behavior or the entanglement entropy of noninteracting 3D fermions as a function of x is given by

$$S_{n,A}(x) = c(n)x^2 \ln x + o(x^2), \tag{100}$$

where

$$c(n) = \frac{1 + n^{-1}}{24(2\pi)^{d-1}} \int_{\partial\Omega} \int_{\partial\Sigma} dS_x dS_k \, |\hat{\mathbf{n}}_x \cdot \hat{\mathbf{n}}_k|, \tag{101}$$

where Ω is the real-space region A scaled to unit volume with normal $\hat{\mathbf{n}}_x$ and Σ is the Fermi volume scaled by the Fermi momentum with unit normal $\hat{\mathbf{n}}_k$. In our case, A is a cubic subsystem (as in Fig. 1) and a spherical Fermi volume.

The noninteracting case is shown in Fig. 11 in two ways. The asymptotic result at large x is shown with crosses on the right edge of the plot, extended into the plot (as a visual aid) with dashed black horizontal lines for $n = 2,3,4,5$ (top to bottom). With a thick red dashed line we show the case $n = 2$ at finite x, as obtained with the overlap-matrix method [60].

Our results for $S_{n,A}$ for the unitary Fermi gas (data points with error bands) appear to heal to the noninteracting limit when the slow decay (see below) to a constant at large x is taken into account; this statement holds especially in the $n = 2$ case where the subleading oscillations allow for a relatively clean fit. Indeed, our fits for $n = 2$ give

$$S_{2,A}(x) = ax^2 \ln x + bx^2, \tag{102}$$

with $a = 0.114(2)$ and $b = 0.04(1)$, while Eq. (101) yields $c(2) = 3/(8\pi) \simeq 0.119366\ldots$. While $c(2)$ are different to within our uncertainties, they are surprisingly close (between 3% and 6%). The subleading behavior is consistent with an area law $\propto x^2$. As n is increased, subleading oscillations become increasingly apparent; however, they are mild enough that it is still possible to discern the asymptotic behavior at large x. For $n = 3,4,5$, oscillations notwithstanding, the results in the large-x limit appear again to be close to the noninteracting case.

Using our results for the entanglement entropies S_n as a function of n, it is possible to use the power method to extract the lowest eigenvalue λ_1 of the entanglement spectrum as a function of x. We studied the decay of $(1 - n)S_n/n$ to a constant value which, given Eq. (98), we identified as $-\lambda_1$. In Fig. 12 we show the result of using that sole eigenvalue to approximate S_n. As expected, higher orders n emphasize the contribution from the lowest entanglement eigenvalue (highest eigenvalue of the reduced density matrix), which progressively dominates S_n as n increases. From the n dependence of S_n,

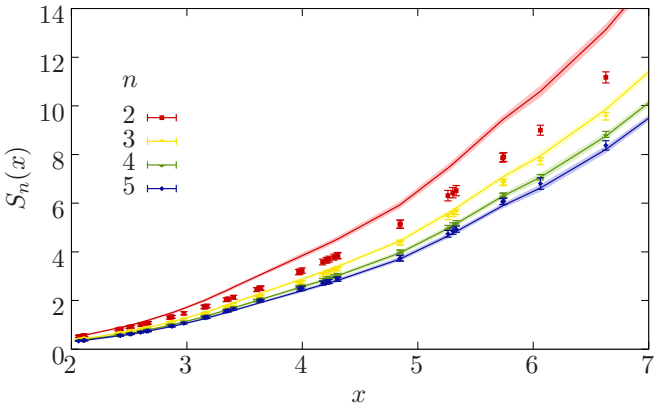

FIG. 12. Rényi entanglement entropy S_n as a function of $x = k_F L_A$ for $n = 2,3,4,5$ (top to bottom). Monte Carlo results are shown as data points with error bars. The solid lines show the result of computing S_n using only the lowest entanglement eigenvalue λ_1, i.e., the approximation $S_n = \frac{n}{n-1}\lambda_1$. Uncertainties appear as shaded regions around the central value.

it is also possible to study the degeneracy of the lowest entanglement eigenstate; at large n,

$$\frac{(1-n)}{n} S_n \simeq \frac{\ln d_1}{n} - \lambda_1 + \cdots , \tag{103}$$

where the ellipsis indicates exponentially suppressed terms, and d_1 is the degeneracy associated with λ_1. We find a vanishing first term, which indicates that d_1 is consistent with unity.

VI. SUMMARY AND CONCLUSIONS

We implemented two different lattice methods to characterize nonperturbatively the entanglement properties of three-dimensional spin-1/2 fermions in the strongly interacting, resonant regime of short interaction range and large scattering length, i.e., the unitary limit. This regime is scale invariant (in fact, nonrelativistic conformal invariant) in the sense that it presents as many scales as noninteracting gases and therefore its properties are universal characteristics of three-dimensional quantum mechanics, i.e., in the same sense as critical exponents that characterize phase transitions.

We analyzed the two-body spectrum of the entanglement Hamiltonian along the BCS-BEC crossover and presented results for the low-lying part, which displays clear features as the strength of the coupling is varied, such as eigenvalue crossing close to the resonance point and merging in the BEC limit. The lowest two eigenvalues in the spectrum correspond to the largest two eigenvalues of the reduced density matrix, which are separated by the Schmidt gap. We found that the latter displays a sharp change at strong coupling, in the vicinity of the conformal point $(k_F a)^{-1} = 0$.

We also carried out a statistical characterization of the high entanglement spectrum, which appears as a quasicontinuum distribution with well defined mean and standard deviation, which we mapped out along the crossover. We found that the mean of the distribution tends to infinity in the noninteracting limit, which indicates that that sector is due to nonperturbative effects in the entanglement Hamiltonian. In contrast, the low-lying part of the spectrum has a finite noninteracting limit. All of the above two-body results were obtained with nonperturbative nonstochastic methods which are easily generalizable to higher particle numbers (as we show analytically and diagrammatically for three particles).

In addition, we studied the Rényi entropies of degree $n = 2$, 3, 4, and 5 of many fermions in the unitary limit, which we calculated using a method recently developed by us (based on an enhanced version of the algorithm of Ref. [56]). We found that, remarkably, the large $x = k_F L_A$ (i.e., subsystem size) limit for those entanglement entropies sets in for x as low as 2.0, which allowed us to characterize the leading and subleading asymptotic behavior using $2 \leqslant x \leqslant 10$. For entropies of order $n > 2$, on the other hand, we found that subleading oscillations are enhanced, but not enough to spoil the visualization of the asymptotic behavior at large x.

Our experience with Monte Carlo calculations of $S_{n,A}$ in 1D gave us empirical indication that the entanglement properties of the unitary Fermi gas might not be too different from those of a noninteracting gas. However, since unitarity corresponds to a strongly correlated, three-dimensional point, that intuition could very well have been wrong. Our calculations indicate that the leading-order asymptotic behavior is approximately consistent with that of a noninteracting system, while the subleading behavior is clearly different.

The recent measurement of the second Rényi entropy of a bosonic gas in an optical lattice [19,20] shows that it is possible to experimentally characterize the entanglement properties of the kind of system analyzed here. Our calculations are therefore predictions for such experiments for the case of fermions tuned to the unitary limit.

ACKNOWLEDGMENTS

This material is based upon work supported by the National Science Foundation under Grants No. PHY1306520 (Nuclear Theory Program) and No. PHY1452635 (Computational Physics Program). We gratefully acknowledge discussions with L. Rammelmüller.

APPENDIX A: EXACT EVALUATION OF THE PATH INTEGRAL FOR FINITE SYSTEMS

In order to illustrate the details as well as the generality of this technique, we evaluate the path integral for a four-component tensor from which each of the above traces may be obtained by suitable index contraction.

To this end, we define

$$R_{ac,bd} = \int \mathcal{D}\sigma \, \boldsymbol{U}[\sigma]_{ab} \, \boldsymbol{U}[\sigma]_{cd}. \tag{A1}$$

We first write out each of the matrices $\boldsymbol{U}[\sigma]$ in its product form. That is, we reintroduce the expression

$$\boldsymbol{U}[\sigma] = \prod_{j=1}^{N_\tau} \boldsymbol{U}_j[\sigma]. \tag{A2}$$

For each contribution to the N-body transfer matrix, exactly N factors of the matrix $\boldsymbol{U}[\sigma]$ appear, and as a result each temporal lattice point appears in the integrand N times. Writing out the

integrand and grouping by time slice, we obtain

$$
\begin{aligned}
R_{ac,bd} &= \int \mathcal{D}\sigma\, \boldsymbol{U}[\sigma]_{ab}\, \boldsymbol{U}[\sigma]_{cd} \\
&= \int \mathcal{D}\sigma (\boldsymbol{U}_1[\sigma]\, \boldsymbol{U}_2[\sigma]\, \ldots\, \boldsymbol{U}_{N_\tau}[\sigma])_{ab} \\
&\quad \times (\boldsymbol{U}_1[\sigma]\, \boldsymbol{U}_2[\sigma]\, \ldots\, \boldsymbol{U}_{N_\tau}[\sigma])_{cd} \qquad \text{(A3)} \\
&= \sum_{\substack{k_1,k_2,\ldots,k_{N_\tau-1} \\ l_1,l_2,\ldots,l_{N_\tau-1}}} \int \mathcal{D}\sigma \left(\boldsymbol{U}_1[\sigma]_{ak_1}\, \boldsymbol{U}_1[\sigma]_{cl_1}\right) \\
&\quad \times \left(\boldsymbol{U}_2[\sigma]_{k_1k_2}\, \boldsymbol{U}_2[\sigma]_{l_1l_2}\right) \ldots \\
&\quad \times \left(\boldsymbol{U}_{N_\tau}[\sigma]_{k_{N_\tau-1}b}\, \boldsymbol{U}_{N_\tau}[\sigma]_{l_{N_\tau-1}d}\right) \qquad \text{(A4)} \\
&= \sum_{\substack{k_1,k_2,\ldots,k_{N_\tau-1} \\ l_1,l_2,\ldots,l_{N_\tau-1}}} \prod_{j=1}^{N_\tau} \left(\int \mathcal{D}\sigma(\tau_j)\, \boldsymbol{U}_j[\sigma]_{k_{j-1}k_j}\, \boldsymbol{U}_j[\sigma]_{l_{j-1}l_j} \right), \\
& \qquad \text{(A5)}
\end{aligned}
$$

where we set $k_0 = a$, $l_0 = c$, $k_{N_\tau} = b$, and $l_{N_\tau} = d$, and used the notation

$$\mathcal{D}\sigma(\tau) \equiv \prod_{\mathbf{r}} \frac{d\sigma(\mathbf{r},\tau)}{2\pi}. \qquad \text{(A6)}$$

Using the specific form of the individual $\mathbf{U}$ factors, we find

$$
\begin{aligned}
&\int \mathcal{D}\sigma(\tau_j) \boldsymbol{U}_j[\sigma]_{k_{j-1}k_j} \boldsymbol{U}_j[\sigma]_{l_{j-1}l_j} \\
&\quad = \sum_{\substack{p,q \\ p',q'}} \int \mathcal{D}\sigma(\tau_j) \left(\boldsymbol{T}_{k_{j-1}p} \boldsymbol{V}_j[\sigma]_{pq} \boldsymbol{T}_{qk_j}\right) \\
&\quad \times \left(\boldsymbol{T}_{l_{j-1}p'} \boldsymbol{V}_j[\sigma]_{p'q'} \boldsymbol{T}_{q'l_j}\right), \qquad \text{(A7)}
\end{aligned}
$$

which using our chosen form of $\mathbf{V}$ becomes

$$
\begin{aligned}
&= \sum_{\substack{p,q \\ p',q'}} \boldsymbol{T}_{k_{j-1}p} \boldsymbol{T}_{qk_j} \boldsymbol{T}_{l_{j-1}p'} \boldsymbol{T}_{q'l_j} \delta_{pq} \delta_{p'q'} \\
&\quad \times \int \mathcal{D}\sigma(\tau_j)(1 + A\, \sin\sigma(p,\tau_j))(1 + A\, \sin\sigma(p',\tau_j)) \\
&= \sum_{\substack{p,q \\ p',q'}} \boldsymbol{T}_{k_{j-1}p} \boldsymbol{T}_{qk_j} \boldsymbol{T}_{l_{j-1}p'} \boldsymbol{T}_{q'l_j} \delta_{pq} \delta_{p'q'} (1 + (e^{\tau g} - 1)\delta_{pp'}),
\end{aligned}
$$

where we used

$$
\begin{aligned}
&\int \mathcal{D}\sigma(\tau_j)(1 + A\, \sin\sigma(p,\tau_j))(1 + A\, \sin\sigma(p',\tau_j)) \\
&\quad = (1 + (e^{\tau g} - 1)\delta_{pp'}). \qquad \text{(A8)}
\end{aligned}
$$

Thus we arrive naturally at the definition

$$[M_2]_{ac,bd} = \mathcal{K}_{ab}\mathcal{K}_{cd} + (e^{\tau g} - 1)\mathcal{I}_{abcd}, \qquad \text{(A9)}$$

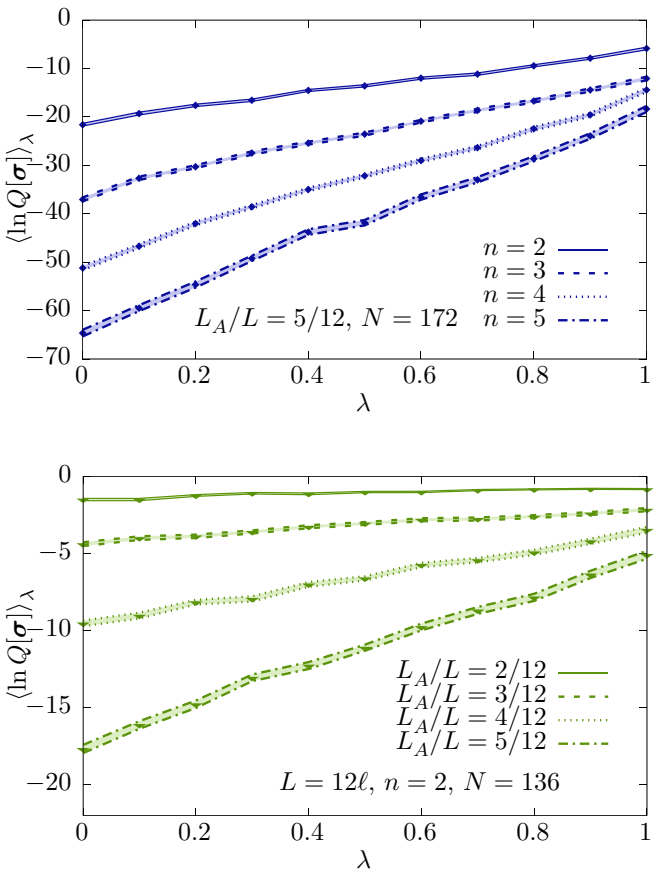

FIG. 13. Top: λ dependence of $\langle \ln Q[\boldsymbol{\sigma}] \rangle_\lambda$ for several Rényi orders $n = 2,3,4,5$, for subsystem size $L_A = 5/12L$, for $N = 172$ fermions at unitarity in a box of size $L = N_x\ell$ (where $N_x = 12$ points and $\ell = 1$). Bottom: λ dependence of $\langle \ln Q[\boldsymbol{\sigma}] \rangle_\lambda$ for several subsystem sizes L_A, for $N = 136$ fermions at unitarity in a box of size $L = N_x\ell$ (where $N_x = 12$ points and $\ell = 1$), and for Rényi order $n = 2$.

as the transfer matrix in the two-particle subspace, where

$$\mathcal{K}_{ij} = \sum_p \boldsymbol{T}_{ip} \boldsymbol{T}_{pj}, \qquad \text{(A10)}$$

$$\mathcal{I}_{ijkl} = \sum_p \boldsymbol{T}_{ip} \boldsymbol{T}_{pj} \boldsymbol{T}_{kp} \boldsymbol{T}_{pl}. \qquad \text{(A11)}$$

Indeed, this definition of M_2 as a transfer matrix makes sense, because

$$R_{ac,bd} = \sum_{\substack{k_1,k_2,\ldots,k_{N_\tau-1} \\ l_1,l_2,\ldots,l_{N_\tau-1}}} \prod_{j=1}^{N_\tau} [M_2]_{k_{j-1}k_j,l_{j-1}l_j}, \qquad \text{(A12)}$$

or more succinctly,

$$R_{ac,bd} = \left[M_2^{N_\tau}\right]_{ac,bd}. \qquad \text{(A13)}$$

In a similar fashion, one may show without much difficulty that the transfer matrix of the three-body problem (for distinguishable particles, i.e., no symmetrization or antisymmetrization is enforced) is

$$[M_3]_{abc,def} = \mathcal{K}_{ad}\mathcal{K}_{be}\mathcal{K}_{cf} + (e^{\tau g} - 1)\mathcal{J}_{abc,def}, \qquad \text{(A14)}$$

where

$$\mathcal{J}_{ijk,lmn} = \mathcal{K}_{il}\mathcal{I}_{jkmn} + \mathcal{K}_{jm}\mathcal{I}_{ikln} + \mathcal{K}_{kn}\mathcal{I}_{ijlm}. \quad \text{(A15)}$$

The pattern from this point on is clearly visible: there is one term for each "spectator" particle that does not participate in the interaction, while the other two are accounted for by an interacting term governed by the $\mathcal{I}_{abcd}$ object. One may thus infer the form of the transfer matrix for higher particle numbers.

APPENDIX B: AUXILIARY PARAMETER DEPENDENCE

In this Appendix we show a few more examples on the mild dependence of the entanglement-entropy derivative $\langle \ln Q[\boldsymbol{\sigma}]\rangle_\lambda$ as other parameters are varied. In all cases, the data shown correspond to full 3D calculations in the unitary regime.

In Fig. 13 (top) we show the variation of that derivative when the Rényi order is changed from $n = 2$ to $n = 5$, at fixed particle number and region size. In Fig. 13 (bottom) we show how $\langle \ln Q[\boldsymbol{\sigma}]\rangle_\lambda$ changes when the particle number is varied, at fixed Rényi order n.

[1] Ultracold Fermi Gases, *Proceedings of the International School of Physics "Enrico Fermi", Course CLXIV, Varenna*, 2006, edited by M. Inguscio, W. Ketterle, and C. Salomon (IOS Press, Amsterdam, 2008).

[2] I. Bloch, J. Dalibard, and W. Zwerger, Many-body physics with ultracold gases, Rev. Mod. Phys. **80**, 885 (2008).

[3] S. Giorgini, L. P. Pitaevskii, and S. Stringari, Theory of ultracold atomic Fermi gases, Rev. Mod. Phys. **80**, 1215 (2008).

[4] M. Lewenstein, A. Sanpera, and V. Ahufinger, *Ultracold Atoms in Optical Lattices: Simulating Quantum Many-body Systems* (Oxford University Press, Oxford, 2012).

[5] M. H. Anderson, J. R. Ensher, M. R. Matthews, C. E. Wieman, and E. A. Cornell, Observation of Bose-Einstein condensation in a dilute atomic vapor, Science **269**, 198 (1995).

[6] C. C. Bradley, C. A. Sackett, J. J. Tollett, and R. G. Hulet, Evidence of Bose-Einstein Condensation in an Atomic Gas with Attractive Interactions, Phys. Rev. Lett. **75**, 1687 (1995).

[7] K. N. Davies, M. O. Mewes, M. R. Andrews, N. J. van Druten, D. S. Durfee, D. M. Kurn, and W. Ketterle, Bose-Einstein Condensation in a Gas of Sodium Atoms, Phys. Rev. Lett. **75**, 3969 (1995).

[8] G. Brumfiel, Focus: Nobel Prize–The Coolest Atoms, Phys. Rev. Focus **8**, 20 (2001).

[9] C. A. Regal, M. Greiner, and D. S. Jin, Observation of Resonance Condensation of Fermionic Atom Pairs, Phys. Rev. Lett. **92**, 040403 (2004).

[10] C. Chin, R. Grimm, P. Julienne, and E. Tiesinga, Feshbach resonances in ultracold gases, Rev. Mod. Phys. **82**, 1225 (2010).

[11] G. Pagano, M. Mancini, G. Cappellini, L. Livi, C. Sias, J. Catani, M. Inguscio, and L. Fallani, Strongly Interacting Gas of Two-Electron Fermions at an Orbital Feshbach Resonance, Phys. Rev. Lett. **115**, 265301 (2015).

[12] M. Höfer, L. Riegger, F. Scazza, C. Hofrichter, D. R. Fernandes, M. M. Parish, J. Levinsen, I. Bloch, and S. Fölling, Observation of an Orbital Interaction-Induced Feshbach Resonance in ^{173}Yb, Phys. Rev. Lett. **115**, 265302 (2015).

[13] S. L. Cornish, Viewpoint: Controlling collisions in a two-electron atomic gas, Physics **8**, 125 (2015).

[14] M. J. H. Ku, A. T. Sommer, L. W. Cheuk, and M. W. Zwierlein, Revealing the superfluid lambda transition in the universal thermodynamics of a unitary Fermi gas, Science **335**, 563 (2012).

[15] E. Cocchi, L. A. Miller, J. H. Drewes, M. Koschorreck, D. Pertot, F. Brennecke, and M. Köhl, Equation of State of the Two-Dimensional Hubbard Model, Phys. Rev. Lett. **116**, 175301 (2016).

[16] N. Gemelke, Viewpoint: A close look at the Fermi-Hubbard model, Physics **9**, 44 (2016).

[17] C. Cao, E. Elliott, J. Joseph, H. Wu, J. Petricka, T. Schäfer, and J. E. Thomas, Universal quantum viscosity in a unitary Fermi gas, Science **331**, 58 (2011).

[18] J. A. Joseph, E. Elliott, and J. E. Thomas, Shear Viscosity of a Unitary Fermi Gas Near the Superfluid Phase Transition, Phys. Rev. Lett. **115**, 020401 (2015).

[19] R. Islam, R. Ma, P. M. Preiss, M. E. Tai, A. Lukin, M. Rispoli, and M. Greiner, Measuring entanglement entropy in a quantum many-body system, Nature (London) **528**, 77 (2015).

[20] A. M. Kaufman, M. E. Tai, A. Lukin, M. Rispoli, R. Schittko, P. M. Preiss, and M. Greiner, Quantum thermalization through entanglement in an isolated many-body system, Science **353**, 794 (2016).

[21] B. Zeng, X. Chen, D.-L. Zhou, and X.-G. Wen, Quantum Information Meets Quantum Matter–From Quantum Entanglement to Topological Phase in Many-Body Systems, arXiv:1508.02595.

[22] *The BCS-BEC Crossover and the Unitary Fermi Gas*, edited by W. Zwerger (Springer-Verlag, Berlin, 2012).

[23] E. Zohar, J. I. Cirac, and B. Reznik, Quantum simulations of gauge theories with ultracold atoms: Local gauge invariance from angular-momentum conservation, Phys. Rev. A **88**, 023617 (2013).

[24] E. Zohar and M. Burrello, Formulation of lattice gauge theories for quantum simulations, Phys. Rev. D **91**, 054506 (2015).

[25] T. Pichler, M. Dalmonte, E. Rico, P. Zoller, and S. Montangero, Real-Time Dynamics in U(1) Lattice Gauge Theories with Tensor Networks, Phys. Rev. X **6**, 011023 (2016).

[26] I. Bloch, J. Dalibard, and S. Nascimbène, Quantum simulations with ultracold quantum gases, Nat. Phys. **8**, 267 (2012).

[27] I. M. Georgescu, S. Ashhab, and F. Nori, Quantum simulation, Rev. Mod. Phys. **86**, 153 (2014).

[28] A. Reiserer and G. Rempe, Cavity-based quantum networks with single atoms and optical photons, Rev. Mod. Phys. **87**, 1379 (2015).

[29] G. A. Baker, Jr., Neutron matter model, Phys. Rev. C **60**, 054311 (1999).

[30] R. F. Bishop, Int. J. Mod. Phys. B **15**, iii (2001); see, in particular, "Many-Body Challenge Problem" formulated by G. F. Bertsch.

[31] D. B. Kaplan, M. J. Savage, and M. B. Wise, A new expansion for nucleon-nucleon interactions, Phys. Lett. B **424**, 390 (1998).

[32] D. B. Kaplan, M. J. Savage, and M. B. Wise, Two-nucleon systems from effective field theory, Nucl. Phys. B **534**, 329 (1998).

[33] K. M. OHara, S. L. Hemmer, M. E. Gehm, S. R. Granade, and J. E. Thomas, Observation of a strongly-interacting degenerate Fermi gas of atoms, Science **298**, 2179 (2002).

[34] D. Eagles, Possible pairing without superconductivity at low carrier concentrations in bulk and thin-film superconducting semiconductors, Phys. Rev. **186**, 456 (1969).
[35] A. J. Leggett, Cooper pairing in spin-polarized Fermi systems, J. Phys. Colloq. (Paris) **41**, C7 (1980).
[36] P. Nozieres and S. Schmitt-Rink, Bose condensation in an attractive fermion gas: From weak to strong coupling superconductivity, J. Low. Temp. Phys. **59**, 195 (1985).
[37] K. Balasubramanian, J. McGreevy, Gravity Duals for Non-relativistic CFTs, Phys. Rev. Lett. **101**, 061601 (2008).
[38] D. T. Son, Toward an AdS/cold atoms correspondence: A geometric realization of the Schrödinger symmetry, Phys. Rev. D **78**, 046003 (2008).
[39] S. Kachru, Viewpoint: Glimmers of a connection between string theory and atomic physics, Physics **1**, 10 (2008).
[40] Y. Nishida and D. T. Son, Nonrelativistic conformal field theories, Phys. Rev. D **76**, 086004 (2007).
[41] L. Amico, R. Fazio, A. Osterloh, and V. Vedral, Entanglement in many-body systems, Rev. Mod. Phys. **80**, 517 (2008).
[42] R. Horodecki, P. Horodecki, M. Horodecki, and K. Horodecki, Quantum entanglement, Rev. Mod. Phys. **81**, 865 (2009).
[43] J. Eisert, M. Cramer, and M. B. Plenio, Colloquium: Area laws for the entanglement entropy, Rev. Mod. Phys. **82**, 277 (2010).
[44] M. Srednicki, Entropy and Area, Phys. Rev. Lett. **71**, 666 (1993).
[45] T. Nishioka, S. Ryu, and T. Takayanagi, Holographic entanglement entropy: An overview, J. Phys. A **42**, 504008 (2009).
[46] R. G. Melko, A. B. Kallin, and M. B. Hastings, Finite-size scaling of mutual information in Monte Carlo simulations: Application to the spin-1/2 XXZ model, Phys. Rev. B **82**, 100409 (2010).
[47] M. B. Hastings, I. González, A. B. Kallin, and R. G. Melko, Measuring Renyi Entanglement Entropy in Quantum Monte Carlo Simulations, Phys. Rev. Lett. **104**, 157201 (2010).
[48] S. V. Isakov, M. B. Hastings, and R. G. Melko, Topological entanglement entropy of a Bose-Hubbard spin liquid, Nat. Phys. **7**, 772 (2011).
[49] M. M. Wolf, Violation of the Entropic Area Law for Fermions, Phys. Rev. Lett. **96**, 010404 (2006).
[50] D. Gioev and I. Klich, Entanglement Entropy of Fermions in Any Dimension and the Widom Conjecture, Phys. Rev. Lett. **96**, 100503 (2006).
[51] P. Calabrese, M. Mintchev, and E. Vicari, Entanglement entropies in free-fermion gases for arbitrary dimension, Europhys. Lett. **97**, 20009 (2012).
[52] W. Ding, A. Seidel, and K. Yang, Entanglement Entropy of Fermi Liquids via Multidimensional Bosonization, Phys. Rev. X **2**, 011012 (2012).
[53] H. Leschke, A. V. Sobolev, and W. Spitzer, Scaling of Rényi Entanglement Entropies of the Free Fermi-Gas Ground State: A Rigorous Proof, Phys. Rev. Lett. **112**, 160403 (2014).
[54] J. E. Drut and W. J. Porter, Hybrid Monte Carlo approach to the entanglement entropy of interacting fermions, Phys. Rev. B **92**, 125126 (2015).
[55] J. E. Drut and W. J. Porter, Entanglement, noise, and the cumulant expansion, Phys. Rev. E **93**, 043301 (2016).
[56] T. Grover, Entanglement of Interacting Fermions in Quantum Monte Carlo Calculations, Phys. Rev. Lett. **111**, 130402 (2013).
[57] M. Lüscher, Volume dependence of the energy spectrum in massive quantum field theories. II. Scattering states, Commun. Math. Phys. **105**, 153 (1986).
[58] M. Lüscher, Two-particle states on a torus and their relation to the scattering matrix, Nucl. Phys. B **354**, 531 (1991).
[59] A. Osterloh, L. Amico, G. Falci, and R. Fazio, Scaling of entanglement close to a quantum phase transition, Nature (London) **416**, 608 (2002).
[60] P. Calabrese, M. Mintchev, and E. Vicari, Entanglement Entropy of One-Dimensional Gases, Phys. Rev. Lett. **107**, 020601 (2011).
[61] B. Swingle, J. McMinis, and N. M. Tubman, Oscillating terms in the Renyi entropy of Fermi liquids, Phys. Rev. B **87**, 235112 (2013).
[62] B. Swingle, Entanglement Entropy and the Fermi Surface, Phys. Rev. Lett. **105**, 050502 (2010).
[63] D. Lee, Lattice simulations for few- and many-body systems, Prog. Part. Nucl. Phys. **63**, 117 (2009).
[64] J. E. Drut and A. N. Nicholson, Lattice methods for strongly interacting many-body systems, J. Phys. G: Nucl. Part. Phys. **40**, 043101 (2013).
[65] F. F. Assaad and H. G. Evertz, Worldline and Determinantal quantum Monte Carlo methods for spins, phonons and electrons, in *Computational Many-Particle Physics*, edited by H. Fehske, R. Shnieider, and A. Weise (Springer, Berlin, 2008).
[66] M.-C. Chung and I. Peschel, Density-matrix spectra of solvable fermionic systems, Phys. Rev. B **64**, 064412 (2001).
[67] I. Peschel, Calculation of reduced density matrices from correlation functions, J. Phys. A **36**, L205 (2003).
[68] S.-A. Cheong and C. L. Henley, Many-body density matrices for free fermions, Phys. Rev. B **69**, 075111 (2004).
[69] F. F. Assaad, T. C. Lang, and F. P. Toldin, Entanglement spectra of interacting fermions in quantum Monte Carlo simulations, Phys. Rev. B **89**, 125121 (2014).
[70] F. F. Assaad, Stable quantum Monte Carlo simulations for entanglement spectra of interacting fermions, Phys. Rev. B **91**, 125146 (2015).
[71] S. Humeniuk and T. Roscilde, Quantum Monte Carlo calculation of entanglement Rényi entropies for generic quantum systems, Phys. Rev. B **86**, 235116 (2012).
[72] P. Broecker and S. Trebst, Rényi entropies of interacting fermions from determinantal quantum Monte Carlo simulations, J. Stat. Mech. (2014) P08015.
[73] L. Wang and M. Troyer, Rényi Entanglement Entropy of Interacting Fermions Calculated Using the Continuous-Time Quantum Monte Carlo Method, Phys. Rev. Lett. **113**, 110401 (2014).
[74] D. J. Luitz, X. Plat, N. Laflorencie, and F. Alet, Improving entanglement and thermodynamic Rényi entropy measurements in quantum Monte Carlo, Phys. Rev. B **90**, 125105 (2014).
[75] M. G. Endres, D. B. Kaplan, J.-W. Lee, and A. N. Nicholson, Noise, Sign Problems, and Statistics, Phys. Rev. Lett. **107**, 201601 (2011).
[76] T. DeGrand, Log-normal distribution for correlators in lattice QCD? Phys. Rev. D **86**, 014512 (2012).
[77] S. Duane, A. D. Kennedy, B. J. Pendleton, and D. Roweth, Hybrid Monte Carlo, Phys. Lett. B **195**, 216 (1987).
[78] S. A. Gottlieb, W. Liu, D. Toussaint, and R. L. Renken, Hybrid-molecular-dynamics algorithms for the numerical simulation of quantum chromodynamics, Phys. Rev. D **35**, 2531 (1987).
[79] G. De Chiara, L. Lepori, M. Lewenstein, and A. Sanpera, Entanglement Spectrum, Critical Exponents, and Order Parameters in Quantum Spin Chains, Phys. Rev. Lett. **109**, 237208 (2012).